Experimental search for double-β decay of ^{100}Mo

M. Alston-Garnjost, B. L. Dougherty,* R. W. Kenney, and R. D. Tripp
Lawrence Berkeley National Laboratory, University of California, Berkeley, California 94720

J. M. Krivicich,† H. W. Nicholson, and C. S. Sutton
Mount Holyoke College, South Hadley, Massachusetts 01075

B. D. Dieterle, S. D. Foltz, C. P. Leavitt, and R. A. Reeder
University of New Mexico, Albuquerque, New Mexico 87131

J. D. Baker and A. J. Caffrey
Idaho National Engineering Laboratory, Idaho Falls, Idaho 83415

(Received 24 April 1996)

No evidence for the neutrinoless double-β decay of ^{100}Mo has been found in a search using a segmented Si(Li) detector with source foils enriched to 97% ^{100}Mo. From an exposure of 0.2664 mole years, and using Bayesian statistics to calculate confidence levels, we find a 68% lower limit on the half-life for the $J^p=0^+\rightarrow 0^+$ transition of 0.22×10^{23} yr. The measured half-life of the two neutrino double-β decay is $0.76^{+0.22}_{-0.14}\times10^{19}$ yr. [S0556-2813(97)05601-X]

PACS number(s): 23.40.Bw, 14.60.Pq, 21.10.Tg, 27.60.+j

I. INTRODUCTION

Since 1930, when Pauli postulated the existence of the neutrino, much effort has been devoted to its investigation, and while we have learned a great deal about the interactions of neutrinos with other particles, our knowledge of its most fundamental properties is essentially rudimentary. The recent search for physics beyond the standard model has resulted in a resurgence of interest in the nature of the neutrino, leading to many experiments on neutrino oscillations, neutrino mass and double-β decay. In this connection, it has long been recognized that neutrinoless double-β decay is the physical process most sensitive to lepton number violation as it pertains to the neutrino. Furthermore, it can be shown within local gauge theories that the neutrino must have a nonzero rest mass for neutrinoless double-β decay to occur [1,2]. Hence detection of neutrinoless double-β decay would be evidence both for massive neutrinos and for lepton number violation.

This paper describes a search for the double-β decay of ^{100}Mo. The experiment uses stacks of thin, disk-shaped Si radiation detectors interleaved with ^{100}Mo foils. This allows us to detect electrons emitted in the decay of a ^{100}Mo nucleus while rejecting other types of background radioactive decay (principally α particles). As previously reported [3,4] we find no evidence for the neutrinoless mode, and now set a lower limit on its half-life of 0.22×10^{23} years.

Double-β decay can only be observed in isotopes in which ordinary β decay is energetically forbidden or highly suppressed. In even-even nuclei the pairing force between like nucleons decreases the ground state energy relative to their odd-odd neighbors. For a given atomic mass number A, when an even-even nucleus of charge $Z+2$ is at a lower energy than a nucleus of charge Z, double-β decay is allowed. If the odd-odd intermediate nucleus of charge $Z+1$ is at a higher energy level, ordinary β decay is forbidden and double-β decay can, in principle, be observed. The situation for ^{100}Mo is shown in Fig. 1. The intermediate ^{100}Tc nucleus has a higher energy than the ^{100}Mo and ^{100}Ru ground states. Double-β decay from ^{100}Mo to ^{100}Ru can be viewed as a second-order process in the Fermi theory of weak interactions, passing through the energetically forbidden ^{100}Tc intermediate state.

Of several possible modes of double-β decay, one which

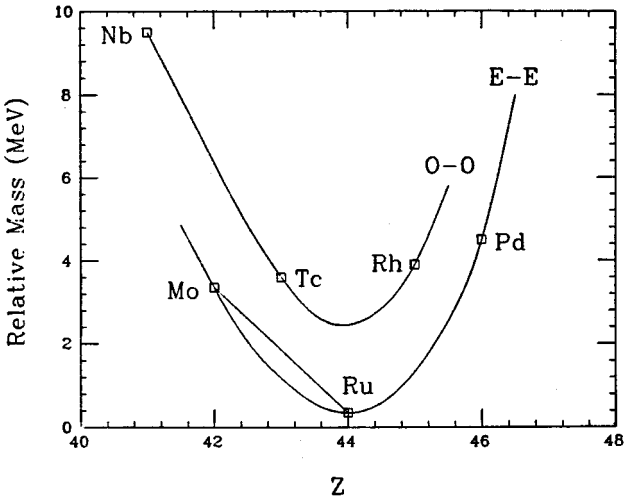

FIG. 1. Relative energies of isobars with atomic weight 100. The ^{100}Mo to ^{100}Tc β decay is energetically forbidden. The double-β decay to ^{100}Ru is allowed.

*Present address: Jet Propulsion Laboratory, 4800 Oak Grove Dr., Pasadena, CA 91109.

†Present address: Joliet Junior College, Department of Natural Science, 1215 Houbolt Rd., Joliet, IL 60431.

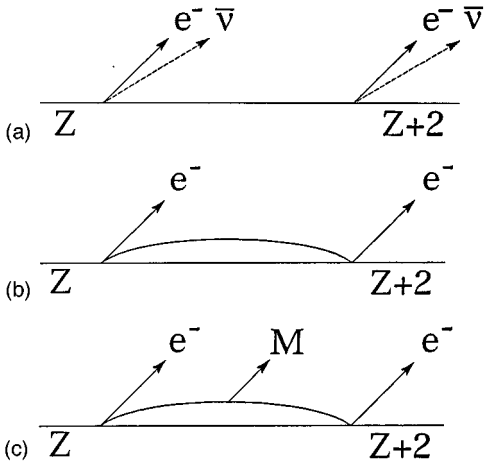

FIG. 2. Diagrams of possible double-β decays. (a) Two neutrino double-β decay. (b) Neutrinoless double-β decay. (c) Majoron decay.

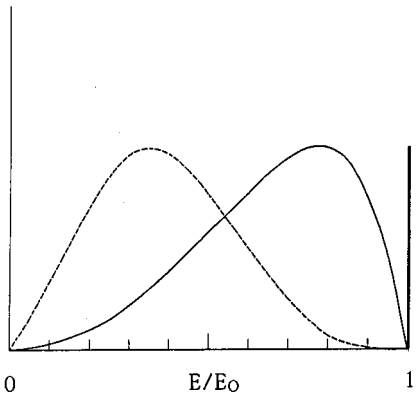

FIG. 3. Sum energy spectra of double-β decays. The dashed line shows the shape of the two neutrino decay, the spike at $E=E_0$ (the total decay energy) is for the neutrinoless decay, and the solid curve is for the Majoron decay. For ^{100}Mo E_0 is 3.033 MeV.

is expected and predictable from Fermi theory, given a knowledge of the nuclear matrix elements, is two-neutrino double-β decay. Here the final state consists of two electrons, two antineutrinos, and a nucleus of charge $Z+2$, as illustrated in Fig. 2(a). Because of its extremely long half-life of order 10^{20} years, it has only recently been detected in the laboratory [5].

The more interesting possibility is neutrinoless double-β decay in which two electrons are emitted without accompanying antineutrinos. This manifestly violates lepton number conservation and can only occur if the electron neutrino is massive and is its own antiparticle, the so-called Majorana neutrino. Electrical neutrality allows this possibility for the neutrino while it is forbidden to other charged leptons and quarks due to their charges. Were it not for the helicity-conserving $V-A$ structure of the weak interaction and the near-zero (or zero) mass of the neutrino, this Majorana neutrino possibility would lead to a much shorter lifetime for the neutrinoless decay mode because the phase space available for the virtual neutrinos in neutrinoless decay far exceeds that for real neutrinos in the two-neutrino mode. The experimental lower limit on the lifetime, being many orders of magnitude greater, would under these circumstances then conclusively favor Dirac neutrinos and lepton number conservation. However the apparent absence of right-handed currents and near-zero mass of the neutrino prevents this conclusion from being drawn unless this mode is actually observed.

In neutrinoless double-β decay [see Fig. 2(b)], the neutrino emitted along with an electron at one interaction vertex is absorbed at the other vertex, where the second electron is produced. For this to occur the neutrino must be its own antiparticle, a Majorana neutrino. In addition, helicity is absolutely conserved for a massless particle undergoing a weak interaction with a $V-A$ structure. If the process occurs via the $V+A$ interaction and only massless neutrinos are involved in the virtual intermediate state, orthogonality between left- and right-handed mixing matrices leads to a zero decay rate [2]. It is thus necessary that there be at least one massive neutrino for the $V+A$ interaction to mediate the process. Therefore detection of neutrinoless double-β decay would be evidence for the existence of massive neutrinos, involving new physics beyond the standard model.

In a third possible decay mode, that of Majoron emission, a conjectured massless Goldstone boson called the Majoron is invoked to generate neutrino mass in much the same way as the Higgs particle generates mass among the other fermions. This leads to the possibility of the Majoron interaction vertex shown in Fig. 2(c). As with two-neutrino double-β decay, only the electrons are observable; the Majoron, like the neutrino, interacts too weakly to be detected.

Experimentally, the three decay modes can be distinguished from each other on a statistical basis by observing the spectrum of the sum of the energies of the two electrons (see Fig. 3). In neutrinoless double-β decay, the two electrons have all the energy and the spectrum has a peak at the ^{100}Mo transition energy of 3.033 MeV. In both the two-neutrino mode and the Majoron mode, the neutrinos or the Majoron, carry off some of the energy and the spectrum for the electrons is determined by four- and three-body phase space, respectively. Figure 3 does not include the effects of energy resolution of the experimental apparatus, or any background the experiment may have.

Table I contains the results of a number of previous investigations of double-β decay.

II. APPARATUS

A. Overview

A detailed description of the apparatus and experimental arrangement in this work have been described elsewhere [6]. Following is a brief overview of the upgraded system used to record the data discussed in this paper.

The experimental approach in the new configuration, as well as its location at a depth of 3300 meters of water equivalent in the Consolidated Silver mine at Osburn, Idaho, remained essentially unchanged. In the apparatus upgrade, important additions and changes to the old system include an increase in the number of detectors and electronic channels to 145 (more than tripling their number) and an increase in complexity of each channel. The upgraded molybdenum foils were changed in form, the computer system software

TABLE I. Partial list of previous experiments.

Element	Group	Technique	$t_{1/2}$ years	
		Two neutrino measurements		
^{76}Ge	PSL/U.So.Carolina[a]	natural Ge detector	$1.1+0.6-0.3\times10^{21}$	
^{76}Ge	K/M-P/A[b]	enriched Ge detector	$1.42\pm0.03(\text{stat})\pm0.13(\text{syst})\times10^{21}$	
^{82}Se	U.C. Irvine[c]	TPC	$1.08+0.26-0.06\times10^{20}$	
^{100}Mo	U.C. Irvine[d]	TPC	$1.16+0.34-0.08\times10^{19}$	
^{100}Mo	Osaka U.[e]	drift chamber	$1.15+0.3-0.2\times10^{19}$	
^{100}Mo	NEMO 2[f]	drift tubes	$0.95\pm0.04(\text{stat})\pm0.09(\text{syst})\times10^{19}$	
^{116}Cd	NEMO 2[g]	drift tubes	$3.6\pm0.6(\text{stat})\pm0.3(\text{syst})\times10^{19}$	
^{116}Cd	ELEGANTS-V[h]		$2.6+0.9-0.5\pm0.35(\text{syst})\times10^{19}$	
^{150}Nd	ITEP/INR/Moscow[i]	TPC	$1.7+1.1-0.6\times10^{19}$	
		Neutrinoless Limits (0^+ to 0^+)		
Element	Group	Technique	$t_{1/2}$ years	C.L.
^{48}Ca	Beijing[j]	CaF_2 scintillator	9.5×10^{21}	76%
^{76}Ge	UCSB/LBL[k]	natural Ge detector	2.4×10^{24}	68%
^{76}Ge	Heidelberg/Moscow[l]	enriched Ge detector	1.93×10^{24}	90%
^{82}Se	U.C. Irvine[c]	TPC	2.7×10^{22}	68%
^{100}Mo	LBL/MHC/UNM/INEL[m]	Si detector	2.2×10^{22}	68%
^{116}Cd	Kiev[n]	CdWO4 scintillator	2.9×10^{22}	90%
^{130}Te	U. Milano/INFN[o]	TeO_2 thermal detector	1.8×10^{22}	90%
^{136}Xe	Neuch./Pasadena/Vill.[p]	TPC	3.7×10^{23}	90%
			2.8×10^{23} (rhc)	90%

[a]H. S. Miley *et al.*, Phys. Rev. Lett. **65**, 3092 (1990).
[b]A. Balysh *et al.*, Phys. Lett. B **322**, 176 (1994).
[c]S. R. Elliott *et al.*, Phys. Rev. C **46**, 1535 (1992).
[d]S. R. Elliott *et al.*, J. Phys. G **17**, S145 (1991).
[e]H. Ejiri *et al.*, Phys. Lett. B **258**, 17 (1991).
[f]D. Dassié *et al.*, Phys. Rev. D, **51**, 2090 (1995).
[g]R. Arnold *et al.*, JETP Lett. **61**, 170 (1995).
[h]K. Kume *et al.*, Nucl. Phys. **A577**, 405 (1994).
[i]V. A. Artem'ev *et al.*, JETP Lett. **58**, 262 (1993).
[j]K. You *et al.*, Phys. Lett. B **265**, 53 (1991).
[k]D. O. Caldwell *et al.*, Nucl. Phys., Proc. Suppl. **B13**, 547 (1990).
[l]H. V. Klapdor-Kleingrothaus, Nucl. Phys., Proc. Suppl. **B31**, 72 (1993).
[m]M. Alston-Garnjost *et al.*, this paper.
[n]F. A. Danevich *et al.*, Phys. Lett. B **344**, 72 (1995).
[o]A. Alessandrello *et al.*, Phys. Lett. B **335**, 519 (1994).
[p]V. Jorgens *et al.*, Nucl. Phys., Proc. Suppl. **B35**, 378 (1994).

was greatly improved and the system automation was expanded and made more reliable.

The upgraded calorimeter comprised 145 Si(Li) solid state detectors, interleaved with thin decay foils of powdered metallic ^{100}Mo contained in thin mylar bags. This assembly was supported in two stacks of approximately equal size. The detectors were operated at about 60 volts, approximately 20 volts in excess of the depletion voltage. In this voltage range they developed no charge multiplication and operated as solid state ionization chambers. The detectors were cooled by liquid nitrogen to reduce their noise to tractable levels.

Each detector was served by its own electronic channel and the data were recorded on disk by a computer located at the underground experimental site. These complete data sets were removed on diskettes only twice weekly, but hourly checks on data accumulation and operational status underground were monitored on the surface, allowing oversight during periods of unattended operation that typically spanned three or four days.

B. Detectors

The detectors were lithium drifted silicon disks of 1.4 mm thickness and 76 mm diameter. A schematic drawing of a detector is shown in Fig. 4. The lithium drifted silicon surface barrier devices were provided with a gold ohmic contact, covering one side, that was conventionally thin (40 μg/cm^2). The surface barrier on the opposite side (moat side) was produced by a 20 μg/cm^2 layer of low radioactivity aluminum deposited on the silicon surface up to a radius just short of a circumferential insulating moat located very close to the outer edge of the device. Thus, the detectors were provided with windows that were extremely thin on both sides, making a detector stack an efficient calorimeter for electrons from the foils.

The detectors were contained in a titanium cryostat and were operated near 120 K in order to reach satisfactorily low noise levels. They were arrayed coaxially in two stacks of 74 and 71 detectors, respectively, with gaps of 1.9 mm between adjacent devices to accommodate the thin Mo decay sources. The stacks were held in place by a rack constructed of OFHC copper which served to constrain the detectors mechanically as well as to provide good heat conduction between each detector and the cooling system. A schematic arrangement is shown in Fig. 4. The detectors were also protected from radiant heating by gold heat shields of 0.125 mm thickness that completely enclosed the detectors and were cooled by the copper rack which, in turn, was in good thermal contact with a heat conducting copper bar whose opposite end was deeply

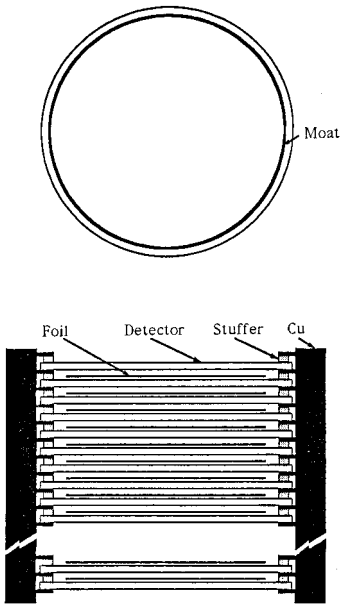

FIG. 4. Schematic of a silicon detector (plan view), and of the detector stack and support structure (elevation).

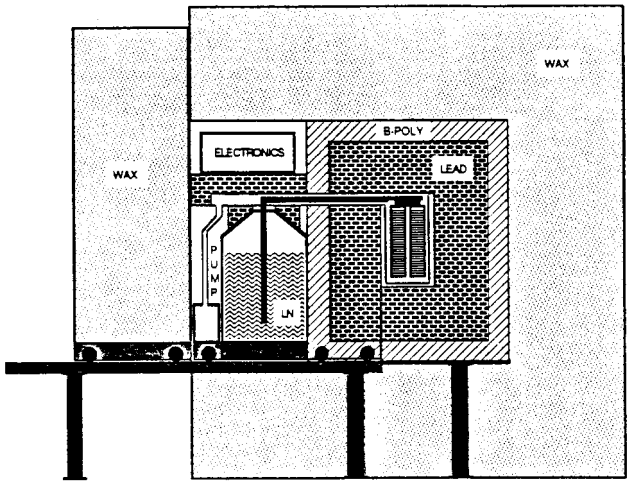

FIG. 5. Schematic elevation of the apparatus and shielding. See Sec. II B for details. The entire system rolled out of the principal shield for component access. This included the cryostat, detectors, lower left quadrant of lead and borated polyethylene shielding, LN dewar, vacuum pump, electronics, the lead shielding beneath the electronics and over the LN dewar, and the outer block of wax shielding. The rails were extended to allow complete access to the detectors.

immersed in a reservoir volume of liquid nitrogen.

Radioactively clean materials were required for constructing this apparatus, particularly for those portions in close proximity to the detectors. It was found that OFHC copper, commercial titanium, and gold were sufficiently free from uranium, thorium, and the members of their radioactive decay chains, to be acceptable. Thus, the rack and heat conducting bar, described above, were of OFHC copper and the cryostat, needed for thermal insulation of the cooled detector array, was constructed of titanium. The welds in the vacuum system were made by using thorium-free welding rods in an inert atmosphere. The heat shields were gold foils for reasons of radioactive cleanliness and very low thermal emittance. The exterior surfaces of the copper rack and heat conducting copper bar were gold plated to minimize their thermal coupling to the room temperature cryostat.

The radioactive isolation of the detector stacks was accomplished by enclosing them and the critical portion of the cryostat within a 25 cm thick shield of low radioactivity lead. This lead house was in turn shielded from neutrons, that issued both from (α,n) reactions and from spontaneous fissions within the environment, by surrounding it with 5 to 10 cm of borated polyethylene that was in turn surrounded by a 56-cm-thick wax neutron moderator. See Fig. 5. The entire assembly was mounted in a deep silver mine at 3300 m.w.e. (meters of water equivalent) in order to avoid cosmic rays. The mine atmosphere was contaminated by radon gas, with a measured activity of approximately 15 pCi/liter of air. The ambient atmosphere was excluded from the central cavity of the lead house by continuously flushing this volume with clean nitrogen gas obtained by boiling liquid nitrogen.

Electrical ground potential and thermal cooling for the detectors were established by having each detector's gold surface in firm contact with the cold copper rack. The copper structure that formed the cooling system then formed the ground potential reference for signals and bias voltages. Pulses from each detector were sensed through a spring contact made directly with the detector's aluminum signal surface. The detector contacts were cut from a 0.25-mm-thick titanium sheet and formed into a sharp pointed spring clamp geometry. In service, the sharp points pressed firmly into the periphery of the aluminum surface where heavy doping of the silicon protected the device from failure even if the aluminum were pierced. The body of the contact was isolated from the detector by an insulating mylar sheet. The electrical connection to the room temperature electronics had to be a good heat insulator as well as a good electrical conductor. This requirement was met by inserting a 2 cm length of #36 stainless steel wire, gold plated for good soldering properties, into the signal lead from each detector. Background from the questionable radioactive contamination of stainless steel was minimized by placing each stainless wire accurately behind the thick copper rack in order to utilize the shielding properties of copper to good advantage. It is suspected that some of the observed background from ^{232}Th may be due to its presence at a level of 4 parts/billion by weight (ppb) in the titanium sheet from which the contacts were made. The solder used on leads near the detectors was certified, by low level-counting, to be free from uranium, thorium, and their decay chain products to levels near one ppb. Signal leads that connected the detectors to the cryostat vacuum feedthrough insulators were polyethylene insulated copper without ground coaxial braids.

C. Molybdenum foils

The newly constituted ^{100}Mo foils were formed of metallic powder contained in thin mylar bags of 6 cm diameter. After undergoing the chemical purification process outlined below, the finely divided molybdenum metallic powder was easy to manipulate physically. It was weighed into approximately one gram lots, each of which was contained in its

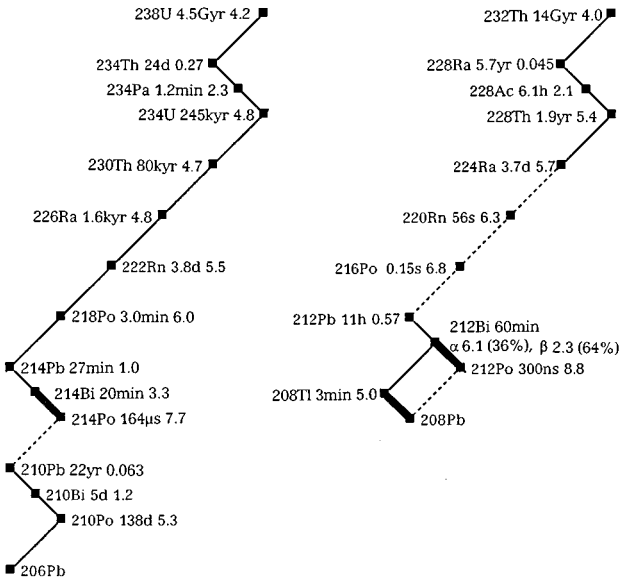

FIG. 6. The naturally occurring radioactive decay chains of ^{238}U and ^{232}Th. Each isotope is listed with its half-life and total decay energy in MeV. (β decays go towards the right and α decays towards the left; heavy lines indicate troublesome β decay backgrounds, and dashed lines indicate α decays used in background studies.)

own flat bag. The bags were made of 4.1-μm-thick mylar sheet and they were closed by peripheral heat welding. Small vents were left open to allow the bags to be exposed to vacuum. The molybdenum powder contained in each bag was rolled flat immediately before being inserted between detectors in the stack. The molybdenum occupied the entire radial space in the bag, and the surface density was approximately 34.4 mg/cm^2, with a point-to-point uncertainty of 10% over the surface area of each foil. The bag and its rolled contents were inserted into the detector stack without disturbing the powdered molybdenum distribution.

The enriched ^{100}Mo used in this work was obtained from Oak Ridge National Laboratory. The first generation of the experiment, as well as neutron activation tests, revealed that the ^{100}Mo sample was contaminated by daughters of the naturally occurring ^{238}U and ^{232}Th decay chains (shown in Fig. 6) at the level of a few ppb. The β decays of the daughter isotopes ^{212}Bi and ^{208}Tl in the Th chain, and ^{214}Bi in the U chain mimicked the double-β decay of ^{100}Mo in the detector stacks. Thus a substantial reduction in this background was necessary to achieve a significant improvement in the half-life limit (4.0×10^{21} yr) for neutrinoless double-β decay established in the first generation of the experiment [3].

A chemical purification process was proposed and tested on normal Mo which had been measured to have contaminations in the U and Th chains on the order of 100 ppb. The measurements were made using gamma spectroscopy. After purification, the level of contamination was below measurable limits ($<$ 1ppb) of U and Th. The success of this program initiated the application of the technique to our supply of enriched ^{100}Mo.

The purification proceeded in the following fashion, taking advantage of the profoundly different chemical behavior of Mo and the actinide series which contains U and Th. In a process quite different from ion exchange, the contaminated Mo powder was dissolved in 2–4 M HNO_3 (M=''molar,'' i.e., 2 to 4 moles of HNO_3 per liter of solution). The solution was boiled to reduce the volume and raise the acidity until Mo formed MoO_3 and precipitated while the actinides that were present stayed in solution. The MoO_3 was then captured in a filter of cellulose nitrate membranes and washed with nano-pure water ($\sim$18 megohm purity). The filter cake was allowed to dry, it was then transferred to a quartz boat that in turn was placed in a quartz tube furnace where the MoO_3 was first dried in a He atmosphere at 150 °C. The atmosphere was then changed to H_2 and the temperature raised gradually to 600 °C to reduce the MoO_3 to Mo. Care was taken in the reduction step because excessively rapid heating can cause MoO_2 to become a vapor while higher temperatures (900 °C) will cause the fine Mo powder to scinter into larger crystals.

Contamination was avoided during the chemical processing by carrying out the entire procedure in a class 10 clean room and by using either quartz or teflon containers. The teflon containers were washed with hot HNO_3/HF to etch the working surfaces in order to remove potential contaminates.

D. Electronics

The complete description of the electronics used to collect the data was published elsewhere [6]. The experiment was controlled by a master computer, an IBM PC/286 at the underground experimental site, whose disk was the depository for the experimental data as well as for the records of the system operation. At approximately hourly intervals, a brief summary of the experimental data was transferred via telephone link to a nearby IBM 286 monitor computer outside the mine, along with a digest of the recent system operational history. This information provided a running record of experimental progress that gave oversight during periods when entry into the mine was not possible.

Access to the experiment was limited by mine schedules to periods of six hours per day, five days per week. Consequently, the entire system was automated to allow unattended operation for up to five days, including complete protection against both power failures and catastrophic equipment failures.

The preamps and shaping amplifiers were custom designed while the remainder of the system was constructed from commercially available CAMAC and NIM modules. System control electronics were unique and therefore custom built.

Each detector fed its own special low-noise charge sensitive preamplifier [7] the output of which was split into two signals, one for amplitude detection and a second one for trigger purposes. Figure 7 is a simplified schematic of a single detector and its associated pair of channels along with the other circuitry common to all detectors. The amplitude (signal) channel output from each detector passed through a relatively slow shaper amplifier. The shaper fed a gated, peak-sensing CAMAC ADC whose digital output was recorded by the master computer. The conversion gain of this preamp and shaper amp system was 270 mV/MeV, where the energy was that lost by a fast electron in silicon.

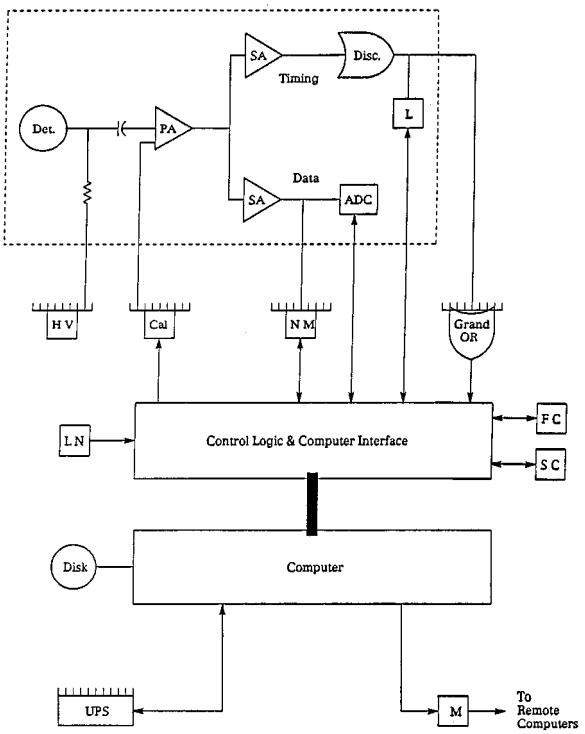

FIG. 7. Schematic of one channel of the electronics and the computer system. See Sec. II D for a review of the system operations. The component identifications are ADC=amplitude to digital converter; Cal=calibration pulser, common to all detectors (lightly coupled); Det=detector; Disc=amplitude discriminator, sets minimum energy deposition for trigger; Disk=data storage disk; FC =fast clock; Grand OR=mixer that serves all channels; HV=high voltage power supply (0–150 volts) common to all detectors; L=latch; LN=liquid nitrogen alarm for low reservoir level; M=modem for communications; NM=noise monitor, reads channels singly; PA=preamplifier; SA=shaper amplifiers, fast in Timing channel, slow in Data channel; SC=slow clock; UPS =uninterruptible power supply.

The system trigger that initiated gating as well as the computer read cycle was derived from that portion of the preamp output found in the trigger channel. In each of these trigger channels a fast rising shaper amplifier output triggered a discriminator if the signal indicated an energy loss in the detector greater than 320 keV and only then were the ADC's gated on. A full computer read cycle followed. As shown in Fig. 7, all detector trigger channels were added in the Grand OR, whose output signal was the system trigger.

The fast clock, having 10 ns resolution, was started by the system trigger and was stopped if a second system trigger was received within the succeeding 50 ms computer readout time. A slow clock, of 1 ms resolution, recorded the time between sequential events. These clocks were read by the computer and their data were incorporated into the subsequent analysis (see Sec. III below).

Each channel was provided with its own latch to identify the detector responsible for any second system trigger received within 50 ms of a first trigger. These latch data were used in the identification of backgrounds.

Control circuitry supervised the experimental operation in a way that protected data and the apparatus against damage from power failures. A fast-toggling battery backup power source maintained the essential electronics and computer in undisturbed operation during power fluctuations or power failures of duration less than 45 minutes. In the case of a more lengthy power failure, or for an essential equipment failure, the data on the underground disk were protected and the surviving apparatus was shut down in a manner that was not destructive.

E. Calibration

The stability of the electronics was assured by calibrating the system before each run, the time interval between calibrations being approximately 75 hours. A computer controlled precision pulser, whose amplitude stability was 25 parts per million (ppm) and whose integral linearity was 50 ppm, generated a program of pulses that spanned the range of detector pulse sizes found in normal operations. These pulses were lightly coupled to each preamp input. The resulting outputs of the ADC's were recorded and used to establish the response function of each channel separately. These response functions were then used in the data reduction process to scale the energy loss in each detector as a function of detector pulse height.

The absolute energy scale of the detector array was established at intervals of approximately six weeks. A ^{228}Th radioactive source of appropriate strength was placed near the detectors in order to expose them to its 2.614 MeV γ ray line. This convenient high energy line arises from the deexcitation of the first excited state of ^{208}Pb, the final (stable) nuclide in the Th decay chain. See Fig. 6. Only single detector electron pair production events were recorded, and the spectral peak resulting from the escape of both positron annihilation photons gave a sharply defined pulse height for the deposition of the remaining 1.593 MeV in each detector (double escape peak). The absolute energy scale, as established by this source calibration procedure, fluctuated by less than 0.2% over the life of the experiment. The calibration routine has been described previously [6,8].

III. EXPERIMENTAL DATA

A. Selection of the experimental data

After each experimental run was concluded, personnel at the mine processed the raw data with the online IBM PC/286 using a simple program. The output from this program together with the online run log were examined to monitor the performance of the equipment. The detector stacks were considered to be functioning properly if the detectors were reasonably quiet and producing triggers. Electronic channels with unusually high or low trigger rates were checked and repaired if possible. A high trigger rate for all detectors was indicative of radon contamination in the cavity within the lead house and required investigation of the liquid nitrogen (LN) purging system.

The raw data for each experimental run were then transferred to VAX computers and input to a preliminary analysis program. This program calculated the energy deposited in each detector using source and electronic calibration data. It also found the total number of detectors containing energy and the total energy for each event, converted the slow and

fast clock times (defined in Sec. II) into seconds, and flagged an event when the energy deposition was in discontiguous detectors. The output from this program constituted a data summary file for each experimental run and was used as input to all subsequent analyses.

In the next stage a second VAX program made histograms and scatter plots which were used to select data for further analyses. The plots were examined to determine the performance of individual detectors, i.e., energy threshold, energy spectrum, and trigger rate. Detectors with zero or abnormally low or high counts, or unusual energy response, were noted for special treatment in subsequent analyses, and were called ''bad'' (See Sec. III C). In addition, a high overall trigger rate vs time, particularly for events with energy below 2 MeV, gave a good indication of radon in the cavity within the lead house. Blocks of data were rejected from the useful data sample if the trigger rate was significantly above average, and the useful live-time for the run was then adjusted. High trigger rates usually occurred for the first few hours after the detector stacks had been retracted from the cavity, (e.g., for a source calibration), and then replaced, or, at the end of an unexpectedly long run when the purging system's LN became exhausted. An indirect file was prepared for each experimental run that selected the desired data from the run data summary file for input to subsequent analyses. Printout of multidetector events with $E>2.5$ MeV from the second VAX program was used to identify zero-neutrino double-β-decay ''candidates'' and helped in the determination of effective cuts.

Additional analyses of the selected data are described in detail below.

B. Triggers

The data for double-β-decay studies of ^{100}Mo were obtained from May 1991 to January 1992. After the data selection described above, the total useful live-time was 3849.5 h. There were 62 foils containing a mass of 60.63 gms of enriched ^{100}Mo (97%) situated above detectors 76 through 137 in stack 2 giving a total useful exposure of 0.2665 mole yr. Stack 1 had no foils in it throughout the exposure.

The electrical contacts to the detectors were rather unreliable. There were four bad detectors in stack 2 for the first 3286.7 hours of the exposure. These runs constituted Experiments 27 through 30 (E27-30). However, after a power failure in November 1991, when vacuum was lost and the cryostat warmed up and had to be recooled, there were eight bad detectors. This latter part of the exposure (E31) corresponded to 562.76 hrs. Stack 1 had 13 bad detectors before the power failure and 19 afterwards. The loss of detectors reduced the detection efficiency for all decays appreciably (see Sec. IV).

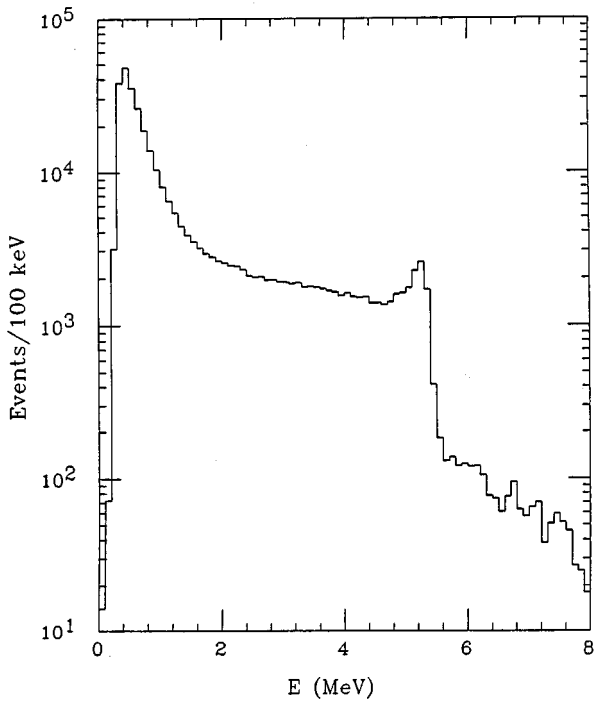

FIG. 8. The energy spectrum (E) of all triggers recorded.

The total number of triggers above a nominal discriminator threshold of 320 keV in the accepted data sample was 299 958, yielding a trigger rate of 78/h. The energy spectrum for these triggers is shown in Fig. 8. Further analysis revealed that about 90% of the triggers had energy recorded in only one detector. The majority of these one detector events above 2.0 MeV were α decays since all naturally occurring α's range out within one detector but electrons with $E>2$ MeV typically deposit energy in two or more detectors. The primary source of the α background was probably the 5.35 MeV decays of ^{210}Po. Figure 8 shows a distinct peak at 5.3 MeV and a large plateau below corresponding to energy-degraded α's. The ^{210}Po contamination probably came from ^{210}Pb in the solder used for electrical connections within the cryostat and was transported to the surfaces of the detectors or surfaces near them by fumes during the soldering operation. At energies below 2 MeV, the triggers were due to energy-degraded α decays and single-β decays from sources within the cryostat, and to γ interactions, mostly Compton scatters, from sources inside and outside the cryostat.

TABLE II. Numbers of observed events and detection efficiencies for neutrinoless double-β decays ($0^+\rightarrow 0^+$ transition) after the cuts described in the text.

Cut	Number of events All energies	Number of events 2.5–3.5 MeV	Detector efficiency 2.5–3.5 MeV (%)[a]
After geom and threshold cuts	147928	7489	54.3
$1<n$det<4	16062	68	43.7
Contiguous energy	12428	57	43.7
''Untagged''	12029	30	43.7
After E cuts	8289	12	35.9

[a]See Sec. IV B.

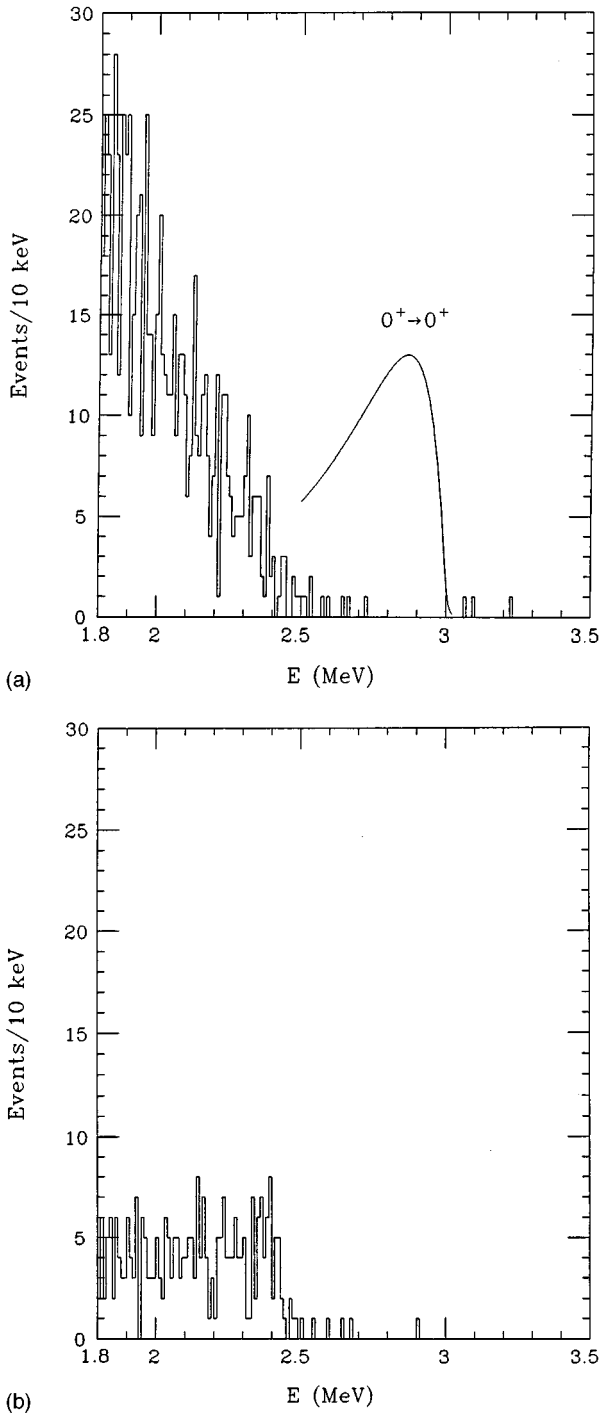

FIG. 9. Energy spectrum of events remaining after all cuts described in Sec. III. (a) For stack 2, detectors 76 → 137, i.e., where there are ^{100}Mo foils. These events are double-β-decay ''candidates.'' The energy spectrum for Monte Carlo generated $0^+ \rightarrow 0^+$ ^{100}Mo double-β decays after the same cuts is shown as a solid line for comparison. This curve is normalized to 500 events. (b) For stack 1, detectors 2 → 73, i.e., where there are no foils.

C. Zero and two neutrino double-β decay ''candidates''

To select the possible double-β-decay ''candidates'' from the background, many cuts on the data were devised by studying Monte Carlo generated events and the real data. The cuts were optimized for the detection of the 0ν double-β-decay transition $0^+ \rightarrow 0^+$, and the rejection of backgrounds, since the investigation of the half-life for this decay was the primary objective of this experiment. The expected backgrounds from the naturally occurring ^{238}U and ^{232}Th decay chains are shown in Fig. 6.

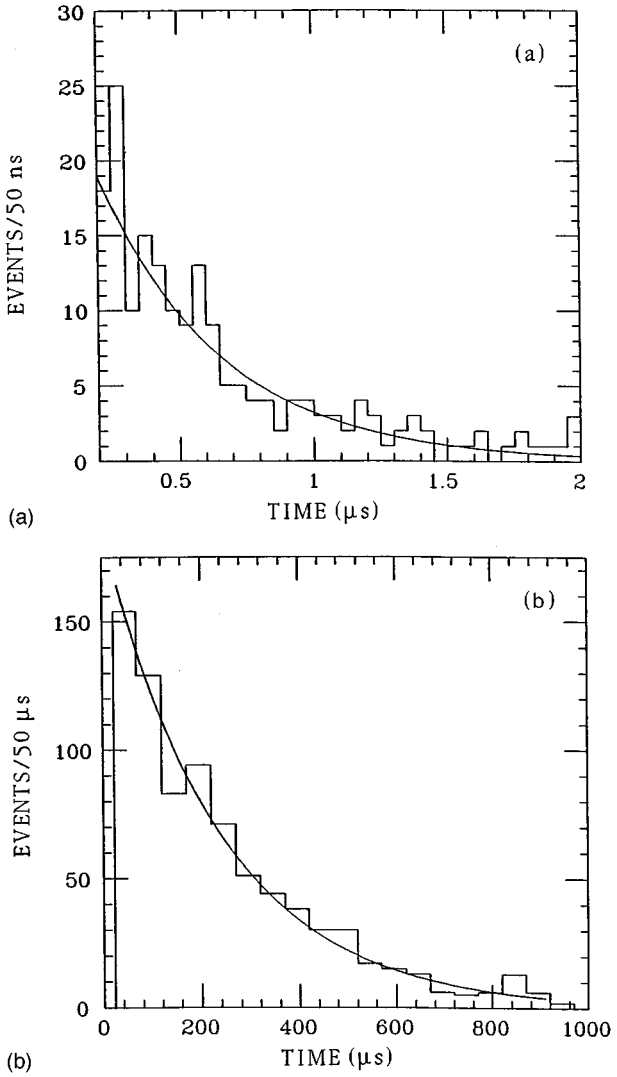

FIG. 10. Time distributions of the α decays of ^{212}Po and ^{214}Po, the daughters of ^{212}Bi and ^{214}Bi, measured by the fast clock. (a) $^{212}\text{Bi} \rightarrow ^{212}\text{Po} \rightarrow ^{208}\text{Pb}$ ($0.2\ \mu\text{s} < t_{\text{fast}} < 2\ \mu\text{s}$). (b) $^{214}\text{Bi} \rightarrow ^{214}\text{Po} \rightarrow ^{210}\text{Pb}$ ($20.0\ \mu\text{s} < t_{\text{fast}} < 1$ ms). The fitted values of the Po decays shown by the solid curves are $t_{1/2}(^{212}\text{Po}) = 0.31 \pm 0.03\ \mu$s and $t_{1/2}(^{214}\text{Po})$ is 0.162 ± 0.007 ms (see text).

The cuts are described below. The number of events remaining after each cut is shown in Table II, for all event-sum-energies (E) and also for $2.5 < E < 3.5$ MeV, the energy region selected for the search for $0^+ \rightarrow 0^+$ zero-neutrino decays.

(1a) To reduce electronic noise, an energy of less than 110 keV recorded in any detector, or energy found in a detector that was known to be bad (noisy or only marginally functional), was ignored and the event-sum-energy and the detector hit multiplicity were adjusted. In addition, for a multidetector event, the energy in a detector was ignored if it was less than 5% of the energy in the detector registering the maximum energy in the event. This cut removed energy

from cross-talk between adjacent channels in the ADC modules.

(1b) The search for double-β-decay ''candidates'' was restricted to the region of stack 2 that contained ^{100}Mo foils, i.e., detectors 76 through 138. Energy in detectors 75 or 139 was used to veto cosmic ray induced events and signals coming from contamination associated with the copper end caps of the stacks.

(1c) Possible ''candidates'' were rejected if they contained energy deposition in a detector that was next to a bad detector, since in this case, the sum energy of the event was suspect.

(2) To remove α decays, all events that contained energy in only one detector were rejected. Events were also rejected if there was energy in four or more detectors because Monte Carlo simulations showed that this cut reduced the number of events from ^{208}Tl and ^{214}Bi β decay backgrounds.

(3) Since single-β decays from the naturally occurring radioactive decay chains are always accompanied by γ deexcitation of daughter states, all events with energy deposited in discontiguous detectors were rejected.

(4) Events ''tagged'' by the fast clock were rejected. These events were beta decays of ^{212}Bi or ^{214}Bi followed by an α decay of the ^{212}Po or ^{214}Po daughter during the 50 msec readout time.

(5a) An additional cut was devised to reduce the number of background events caused by a ^{212}Bi decay followed by an α decay of the ^{212}Po daughter ($t_{1/2}=300$ ns). If the α reached a detector before the trigger system had recovered (about 200 ns) the fast clock was not stopped but the α's energy was recorded in an ADC. An examination of the ''tagged'' ^{212}Bi events showed that most of them had energy in only two detectors, and given that the α deposited energy in only one detector, these events favored unequal energy deposition in the two detectors. Events were rejected from the ''candidate'' sample when the ratio of the energy deposited in the two detectors (Emin/Emax) was less than 1/3.

(5b) For 3 detector events, the energy deposition in the middle detector had to be greater than 450 keV, i.e., the most probable minimum energy deposited by an electron in a detector. This cut reduced the number of single-β-decay events where an associated γ interacted close to the β.

The energy spectrum of the 728 events remaining after all cuts and with energy above 1.8 MeV is shown in Fig. 9(a). These are the double-β-decay ''candidates.''

D. Events detected in stack 1

The data from stack 1, detectors 1-74, from the exposure described in Sec. III A above were analyzed with the same program used to select double-β-decay ''candidates'' in stack 2. In stack 1 the acceptable detector region extended from detector 2 to detector 73. Detectors 1 and 74 were used as vetoes. The 280 events with energy greater than 1.8 MeV that remained after all cuts are shown in Fig. 9(b). Since there was no ^{100}Mo in stack 1, these events gave some indication of the number of background events in stack 2. However, the energy scale, detector multiplicity and detection efficiency were different since an electron typically lost about 100 keV in the foils. A comparison of the stack 1 and 2 data is discussed in detail in Appendix A.

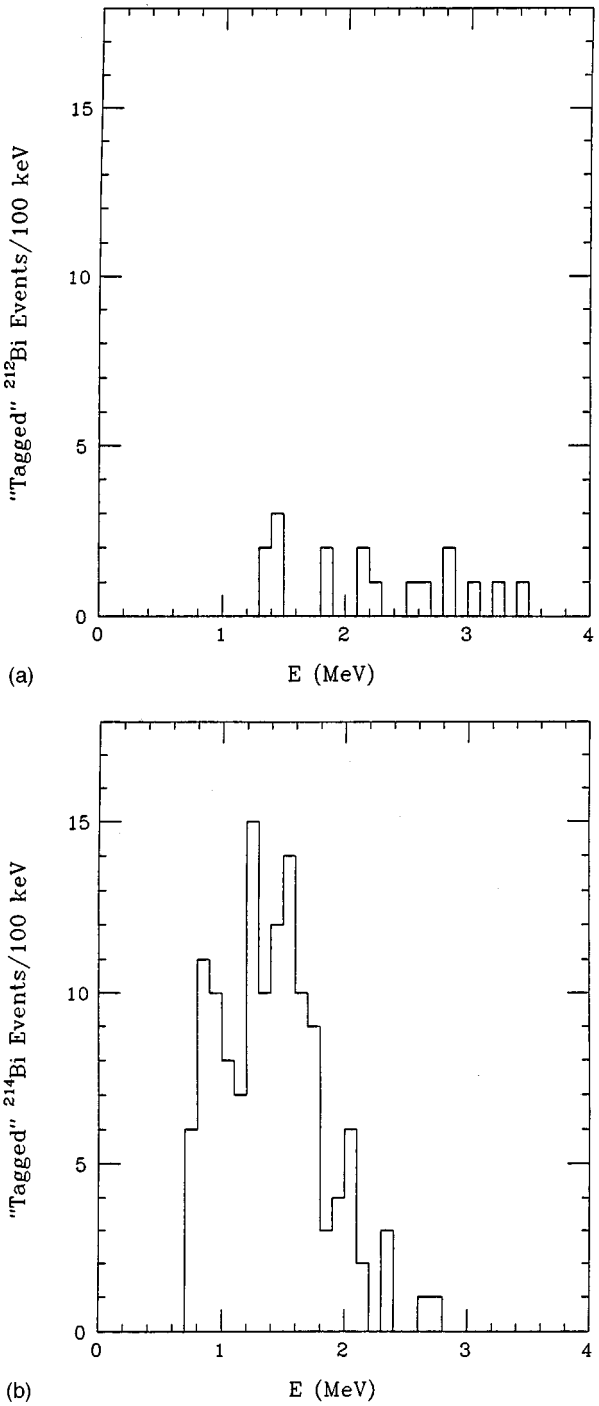

FIG. 11. Energy distributions of the decays of Bi ''tagged'' by the fast clock that remain after all the cuts described in Sec. III. (a) ^{212}Bi decays. (b) ^{214}Bi decays.

E. Events ''tagged'' by the fast clock

Events were ''tagged'' by the fast clock if a second trigger arrived at a detector during the event readout time, provided that this second trigger arrived after the trigger system had recovered and with an energy above the discriminator threshold of approximately 320 keV. These ''tagged'' events were used to estimate contamination of the ''candidate'' sample from the β decays of ^{212}Bi in the ^{232}Tl decay chain, and ^{214}Bi in the ^{238}U decay chain.

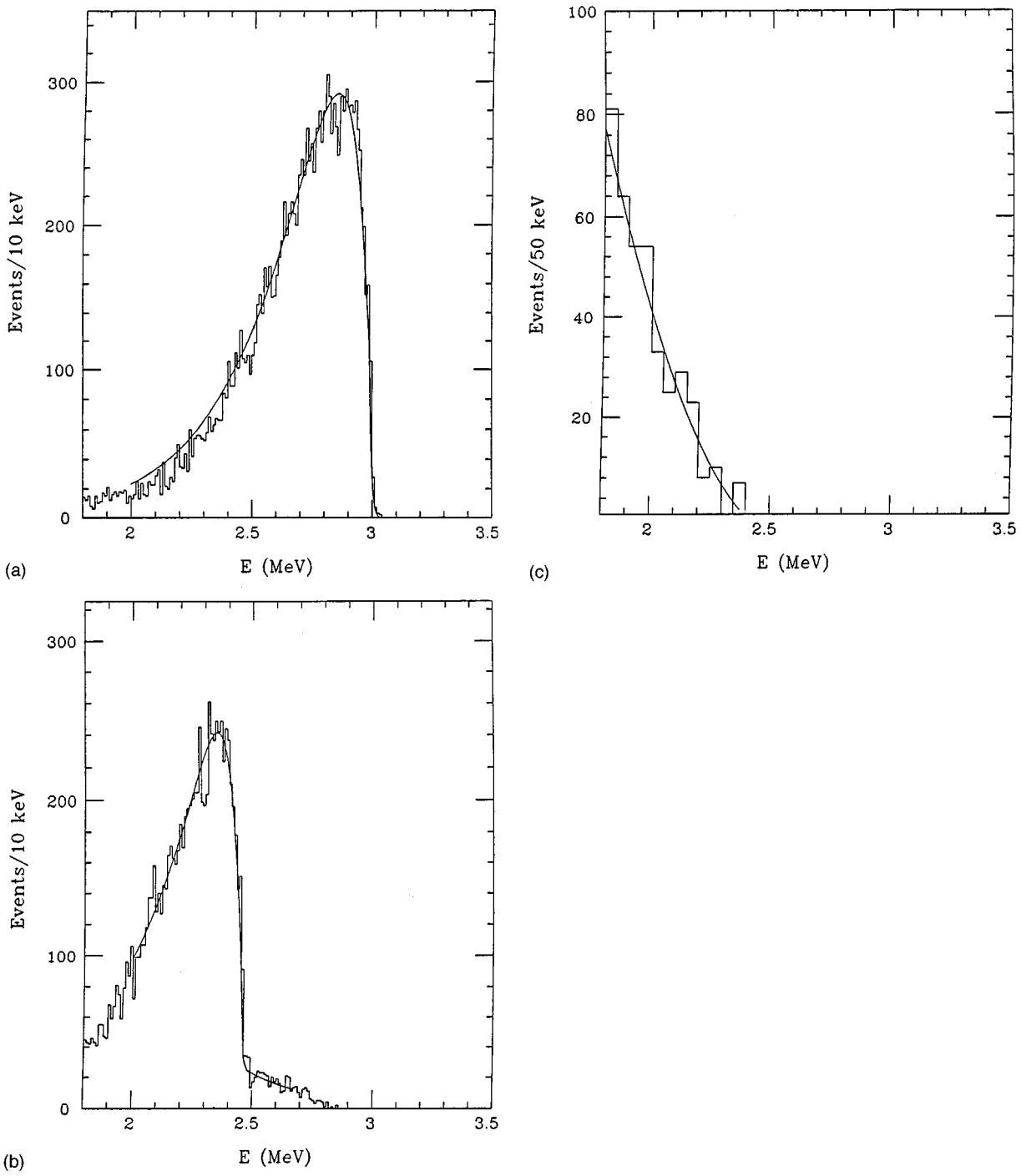

FIG. 12. The energy spectra, after all cuts, of Monte Carlo generated double-β decays of ^{100}Mo (signal) occurring in the foils. (a) Zero neutrino $0^+ \rightarrow 0^+$ transition. (b) Zero neutrino $0^+ \rightarrow 2^+$ transition. (c) Two neutrino decay. The curves are the fitted parametrizations described in Appendix B.

(1) $^{212}\mathrm{Bi} \xrightarrow{\beta} {}^{212}\mathrm{Po}$ ($t_{1/2}=0.3\ \mu$s) $\xrightarrow{\alpha} {}^{208}\mathrm{Pb}$ ($E_\beta=2.3$ MeV, $E_\alpha=8.8$ MeV) ,

(2) $^{214}\mathrm{Bi} \xrightarrow{\beta} {}^{214}\mathrm{Po}$ ($t_{1/2}=164\ \mu$s) $\xrightarrow{\alpha} {}^{210}\mathrm{Pb}$ ($E_\beta=3.3$ MeV, $E_\alpha=7.7$ MeV).

The event sample used to study the ''tagged'' events was from the first 3286.7 hours of the exposure described in Sec. III A above (i.e., E27-30). Cut (1a) described above was made on the data to remove electronic noise from the event sample.

(1) Events were accepted as ^{212}Bi decays followed by the α decay of ^{212}Po, if the fast clock time was between 200 ns and 2 μs. The time distribution for these events is shown in Fig. 10(a) and has a fitted ^{212}Po half-life of $0.31 \pm 0.03\ \mu$s, in good agreement with the accepted value of 0.3μs [9].

(2) For ^{214}Bi decays, the fast clock time was required to be between 20 μs and 1 ms. An additional cut was imposed that required that at least one detector had an energy greater than 0.5 MeV deposited in it. The time distribution for these decays is in Fig. 10(b). The fitted ^{214}Po half-life is

0.162 ± 0.007 ms, in agreement with the accepted value of 0.164 ms [9].

There were 259 ^{212}Bi and 979 ^{214}Bi ''tagged'' events observed in the detectors. After the cuts described in Sec. III B above, but excluding cut 4 (fast clock ''tag''), 17 and 132 events respectively remained for detectors 76-138. The energy spectra of these events are shown in Figs. 11(a) and 11(b). Both of these energy spectra can be used to estimate contributions to the observed double-β-decay ''candidate'' energy spectrum, although the normalization is hard to determine.

F. Multi-α-decay sequences

Multi-α-decay sequences can be used to estimate the number of decays from the ^{232}Th decay chain. These sequences were from the α decays:

$$^{224}\mathrm{Ra} \xrightarrow{\alpha_1} {}^{220}\mathrm{Rn}(t_{1/2}=56\,\mathrm{sec}) \xrightarrow{\alpha_2} {}^{216}\mathrm{Po}(t_{1/2}=0.15\,\mathrm{sec}) \xrightarrow{\alpha_3} {}^{212}\mathrm{Pb}$$

($E_{\alpha_1}=5.7$ MeV, $E_{\alpha_2}=6.3$ MeV, $E_{\alpha_3}=6.8$ MeV)

The event sample used for this search was also the first 3286.7 hours of the exposure described in Sec III A above. Cut (1a) was imposed to remove electronic noise from the event sample.

These α-α and α-α-α decay sequences were detected as two or three separate one detector events. The time separation between the events was measured by the slow clock. For the ^{216}Po decay, a time interval of 0.1 to 1.0 sec was used, and, for the ^{220}Rn decay, 1.0 to 200.0 sec. Events with $E<2.0$ MeV were rejected to maximize the probability that the accepted events were α decays. To detect three-α-decay sequences, the data were first examined for two α sequences from ^{216}Po decays and then preceding events were searched for the ^{220}Rn decay. A total of 86 three-α-decay sequences were found and 204 two decay sequences. Further analysis of these data is described in Appendix A.

IV. MONTE CARLO SIMULATIONS

A. Monte Carlo simulation of events

The CERN program GEANT 3.11 [10] was used to simulate both signal and background decays. The program was first modified to generate the double-β decays of ^{100}Mo, and also the expected backgrounds from the β decays, and subsequent γ deexcitations, of radioactive isotopes in the naturally occurring ^{238}U and ^{232}Th chains (See Fig. 6). The program was also modified to track the dE/dx and multiple scattering of low energy electrons through the geometry of this experiment. The simulated Monte Carlo data for simple experiments was compared with published results: e.g., practical ranges and backscattering of electrons with energies of 50 keV to 5 MeV incident normally on silicon, and also dE/dx of electrons, and γ-ray attenuation lengths in both Si and Mo. The agreement was good in all cases [11].

For simulated signal and background decays, particles were tracked through the detector stacks and the energy deposited in the sensitive region of each detector was recorded in a format identical to that of real events. These simulated events were subsequently processed by the same programs used for the experimental data, including all the cuts described earlier. This gave calculated detection efficiencies for signal and background events, as well as the expected shapes of the energy spectra. These spectral shapes were fitted by algebraic expressions (see Appendix B) and used in the analysis described in detail in Sec. VI.

B. Signals

Simulated signal events from ^{100}Mo sources situated within the foils were generated for zero-neutrino double-β decays ($0^+ \rightarrow 0^+$ and $0^+ \rightarrow 2^+$ transitions) and for two-neutrino decays. The resulting energy spectra for these signals are shown in Figs. 12(a)–12(c), together with curves representing the fitted parametrizations. Thirty thousand events were generated for each of the two 0ν transitions, and twenty thousand for the 2ν decay.

The simulations of zero-neutrino double-β-decays showed that the width of the 0ν peak varied dramatically depending on the ^{100}Mo foil thickness. This is only partly due to the energy lost by the electrons within the foils. Backscattering from the silicon detectors significantly enhances this effect. In addition, because scattering is so dominant, any signal characteristics that might arise from angular correlations of the double-β decay electrons is lost.

In Table II the calculated detection efficiencies for $0^+ \rightarrow 0^+$ 0ν decays in the energy region $2.5<E<3.5$ MeV are shown, after imposing all of the cuts described earlier. This table reveals how such cuts are effective at reducing the data sample much more than the calculated efficiency for observing a signal.

Detection efficiencies for the three signals are shown in Table III, after all cuts are applied, and for the energy regions where this experiment is expected to be most sensitive. It can be seen that the loss of useful detectors greatly reduces the detection efficiencies. This is evident in the decrease in

TABLE III. Calculated detection efficiency for double-β decays.

Expt.	Live-time (hr)	Live-time (mole-yr)	Efficiency (%) (2.5 → 3.5 MeV) 0ν, $0^+ \rightarrow 0^+$	Efficiency (%) (2.1 → 2.5 MeV) $0\nu, 0^+ \rightarrow 2^+$	Efficiency (%) (1.9 → 2.5 MeV) 2ν
27–30	3286.7	0.2275	37.0 ± 0.4	23.5 ± 0.3	1.23 ± 0.08
31	562.8	0.0390	29.4 ± 0.3	18.8 ± 0.3	1.02 ± 0.07
			Totals		
27-31	3849.5	0.2665	35.9 ± 0.4	22.8 ± 0.3	1.20 ± 0.08

efficiencies when there are eight bad detectors in stack 2 (as in E31), compared to data taken when four bad detectors were present (E27-30).

C. Backgrounds

The most troublesome backgrounds are β decays of ^{212}Bi and ^{208}Tl in the ^{232}Th decay chain, and ^{214}Bi in the ^{238}U chain.

To investigate these backgrounds from sources within the ^{100}Mo foils, 20 000 events were generated from each isotope. These events included the electron and associated deexcitation γ's. The generated energy spectra for ^{208}Tl and ^{214}Bi are shown in Figs. 13(a) and 13(b) together with the fitted curves. The generated spectrum for ^{212}Bi decays (not shown) extends only to 2.1 MeV as expected. This shows that energy from a subsequent α decay of the ^{212}Po daughter that occurs during the recovery time of the trigger system must be recorded in an ADC for the total energy of a real event to be greater than 2.1 MeV.

Backgrounds from sources outside the foils are due to the interaction of high-energy γ's in the foils and detectors. Such backgrounds become important for event energies below about 2.4 MeV. The Compton edge for the scattering of the 2.614 MeV γ's from ^{208}Tl is at 2.38 MeV, and at 2.22 MeV for 2.445 MeV ^{214}Bi γ's. The locations of these radioactive sources are unknown. To approximate this situation, 10 000 events coming from each of five different point sources, four outside and one in the middle of the cryostat, were generated for both ^{208}Tl and ^{214}Bi, i.e., totals of 50 000 2.614 MeV and 50 000 2.445 MeV γ's. The energy spectra and the fits to these spectra are shown in Figs. 14(a)–14(d).

V. BACKGROUNDS

A. Expected backgrounds

For energies above 2.0 MeV, the predominant backgrounds contributing to the double-β decay ''candidate'' sample are expected to be from β decays, and the interactions of γ rays, coming from the naturally occurring radioactive decay sequences of ^{238}U or ^{232}Th. These decay sequences are shown in Fig. 6 and in Table IV. In an attempt to estimate the number of background events in the ''candidate'' sample, the events ''tagged'' by the fast clock and the two- and three-α-decay sequences from E27-30 were studied and a comparison was made of the number of events in stack 1 with stack 2. (See Appendix A for details.) For these data, there were 62 good detectors and no foils in stack 1, and 61 good detectors and 62 foils in stack 2. Although the detection efficiencies for the two stacks were not the same, they should be sufficiently similar to make this comparison useful. The detection efficiencies for β's or α's could not be calculated accurately because the location of the radioactive sources relative to the sensitive regions of the detectors were not known. Since the range of α's is small, less than the thickness of a foil, the detection of α's was very sensitive to the location of the sources and the presence or absence of foils.

B. Estimated number of background events

Using the normalization factors obtained in Appendix C, an estimate of the number of background β decays in the sample of double-β-decay ''candidates'' for $E>2.0$ MeV was made. The number of ''untagged'' Bi decays was obtained from the number of ''tagged'' events, and the number of ^{208}Tl events from Monte Carlo simulation. The results are in Table V. This table shows that all the events in the ''candidate'' sample above 2.5 MeV can be easily explained by contributions from ^{212}Bi and ^{214}Bi β decays. Below 2.4 MeV interactions of γ's from ^{214}Bi and ^{208}Tl decays from sources inside or outside the cryostat are expected.

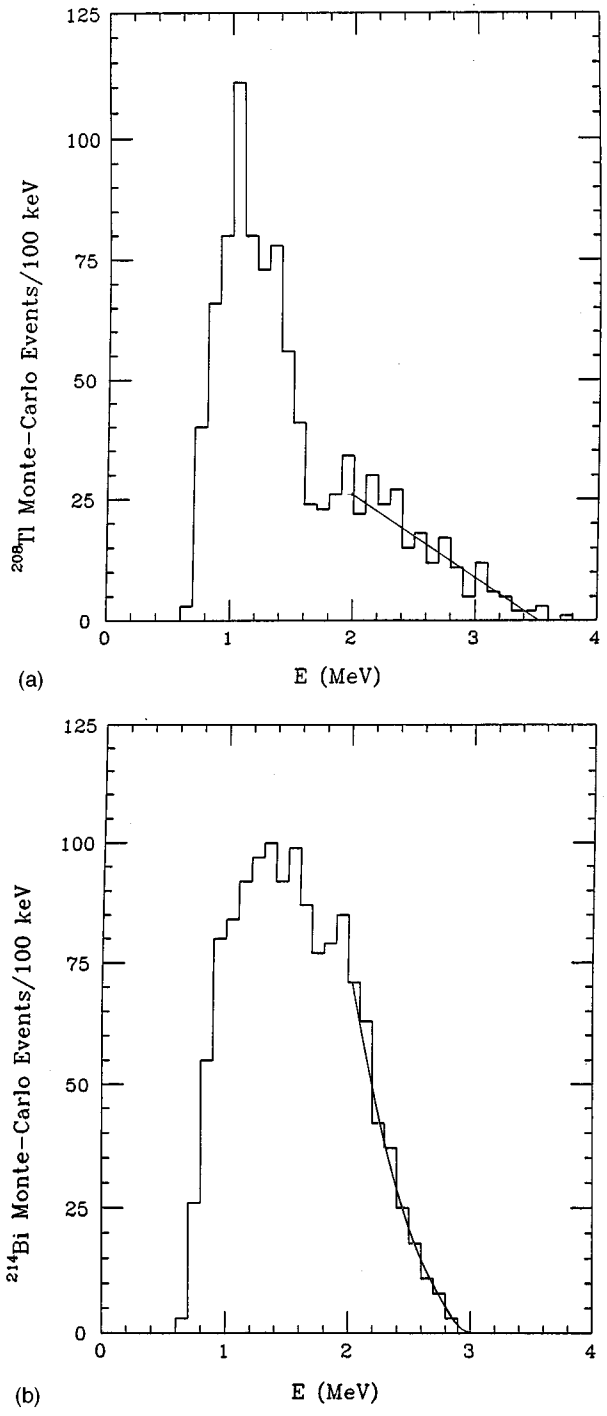

FIG. 13. The energy spectra, after all cuts, of Monte Carlo generated β decays (background) from sources within the foils. (a) β decays of ^{208}Tl. (b) β decays of ^{214}Bi.

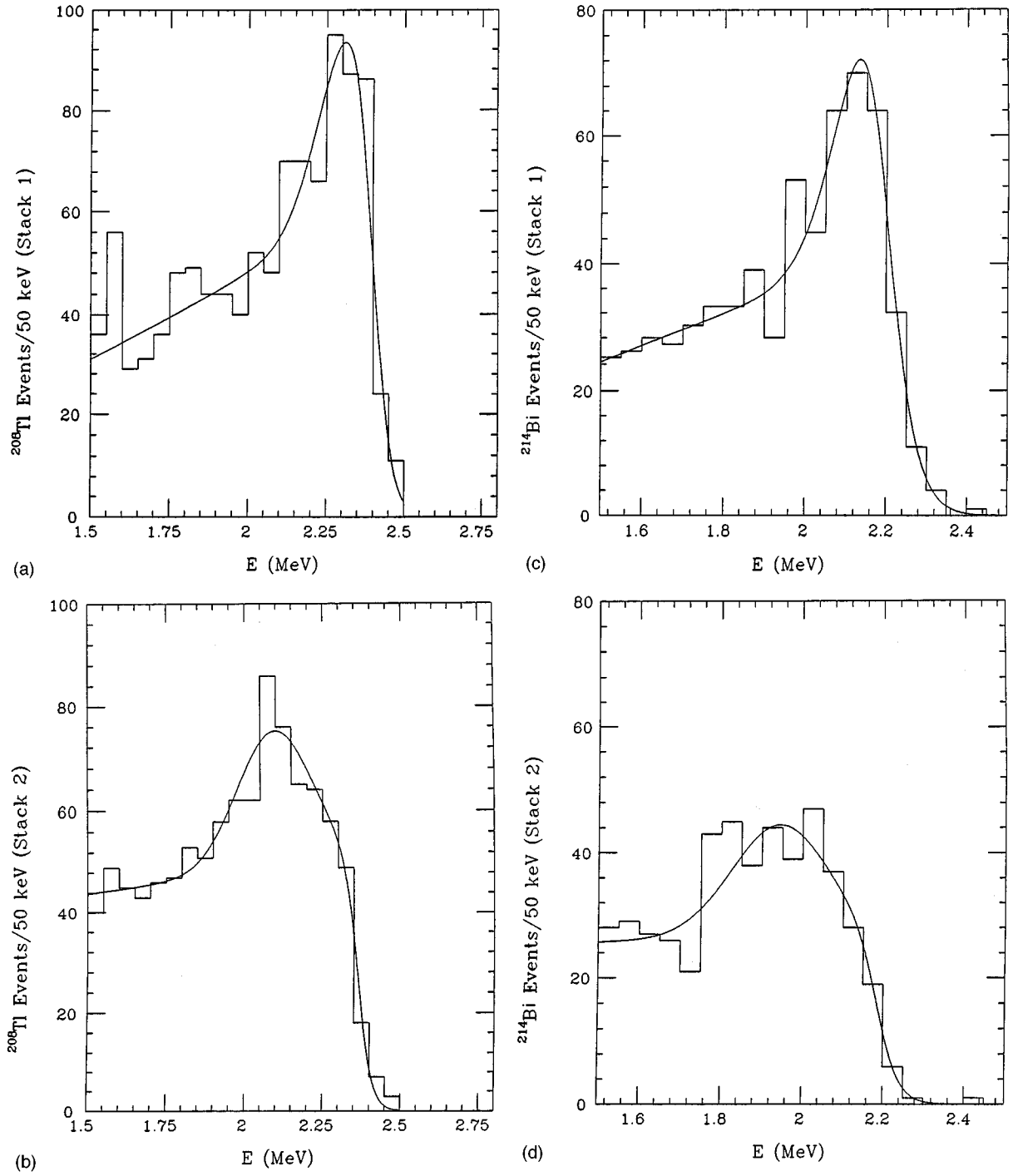

FIG. 14. The Monte Carlo generated energy spectra, after all cuts, of γ's from sources outside the foils that interact in or near the detectors. (a) and (b) Backgrounds in stacks 1 and 2 from the interactions of 2.614 MeV γ's from the β decays of ^{208}Tl. (c) and (d) Backgrounds in stacks 1 and 2 from the interactions of 2.445 MeV γ's from the β decays of ^{214}Bi.

VI. FITS TO THE EXPERIMENTAL ENERGY SPECTRA

A. Fits to the energy spectra for $0^+ \rightarrow 0^+$ zero neutrino decays

In order to obtain a lifetime limit for $0^+ \rightarrow 0^+$ neutrinoless double-β decay, an extended maximum likelihood method was used to estimate the number and error in the number of signal events contained in our data sample [12]. The extended likelihood function can be written

$$\mathcal{L}_{\mathcal{E}} = \frac{e^{-\mu}\mu^n}{n!}\mathcal{L},$$

where $\mu = s + b$, s, and b are the means of the Poisson distributions for signal and background, and n is the number of observed events. $\mathcal{L}$ contains the shape information of the observed energy spectra and is given in our experiment by

TABLE IV. Expected signals and backgrounds.

E (MeV)	Signals	Backgrounds	
2.0→2.5	0ν $0^+\rightarrow 0^+$	β decays	^{212}Bi ($+\alpha$ energy)
	$0^+\rightarrow 2^+$		^{214}Bi
	2ν		^{208}Tl
		γ interactions	2.445 MeV from ^{214}Bi
			2.614 MeV from ^{208}Tl
2.5→3.0	0ν $0^+\rightarrow 0^+$	β decays	^{212}Bi ($+\alpha$ energy)
			^{214}Bi
			^{208}Tl
3.0→3.5		β decays	^{212}Bi ($+\alpha$ energy)
			^{208}Tl

$$\mathcal{L}=\prod_{i=1}^{12}\{f_1\mathcal{P}_{\text{signal}}(E_i)+f_2\mathcal{P}_{\text{Bi212}}(E_i)+f_3\mathcal{P}_{\text{Bi214}}(E_i)+f_4\mathcal{P}_{\text{Tl208}}(E_i)\}.$$

In the expression for $\mathcal{L}$, the functions $\mathcal{P}_j(E_i)$ are the fits to the shapes of signal and background normalized to unity over the energy interval $2.50<E<3.50$ MeV, and the f_j are the statistical fractions of signal and background in each event described in Appendix B. The functions $\mathcal{P}_j$ in the sum are evaluated at the energy E_i of the ith event, and the product is over the 12 events observed in the energy interval between 2.50 and 3.50 MeV. The energies of the individual events (E_i) and the functions $\mathcal{P}_j(E_i)$ are shown in Table VI and Fig. 15, and a three dimensional plot of $\mathcal{L}_\mathcal{E}$ in Fig. 16.

The function $-\ln\mathcal{L}_\mathcal{E}$ is then minimized using MINUIT [13] in terms of the parameters $s=\mu f_1$ and $b_j=\mu f_j$, $j>1$, which correspond to the number of signal and background events, respectively, in the sample when the extended likelihood function is maximized, and the signal is restricted to zero or positive values. For a variety of s and b_j starting values, including minimizations in which one or two of the background b_j's are held constant or at zero, the negative log likelihood function is always minimized when s is pushed to zero with a one-sided error of 0.917 events or less. This procedure corresponds to finding σ in the analogous Gaussian case. The fitted values of the backgrounds are ^{212}Bi $=4.1$ events and ^{214}Bi$=7.9$ events with ^{208}Tl fixed at 0.0 events.

Based on this analysis, a 68% confidence limit on the $0^+\rightarrow 0^+$ neutrinoless double-β decay can be obtained from the formula

$$t_{1/2}\geqslant\frac{\ln(2)\times\epsilon_0 T\times N_a}{s_0}$$

where $\epsilon_0 T=0.36\times 0.2664=0.0959$ mole-yr is the product of the detector efficiency and live-time, N_a is Avagadro's number, and s_0 is the number of neutrinoless double-β-decay events. Using 0.917 for s_0, we obtain $t_{1/2}>0.437\times 10^{23}$years. This value has been reported previously [4].

It should be pointed out, however, that the above confidence limit is based on a fit to our data *only* and is a statement about the number of signal events observed. To obtain a confidence limit based on Poisson statistics about how likely such a result would be obtained in repetitions of identical experiments, we have used a Bayesian procedure based on a method given in a recent paper by Innocente and Lista [14]. In this method, the extended likelihood function is integrated to obtain an upper limit of the number of events (l) corresponding to various confidence levels.

The normalized extended likelihood function $\mathcal{L}_n$ is given by

$$\mathcal{L}_n=\mathcal{N}\frac{e^{-(b+s)}(b+s)^n}{n!}\Pi_{i=1}^n[f_b\mathcal{P}_b(E_i)+f_s\mathcal{P}_s(E_i)],$$

where $\mathcal{N}$ is the normalization constant defined such that

$$\int_0^\infty\mathcal{L}_n ds=1.$$

TABLE V. Estimated backgrounds from ^{212}Bi, ^{214}Bi, and ^{208}Tl β decays within the cryostat.

		^{208}Tl			Measured
E (MeV)	^{212}Bi	min	max	^{214}Bi	(total)
2.0→2.5	1.9 ± 0.6 [a]	0	3.5	45.9 ± 11.9 [a]	349.0 ± 18.7
2.5→3.0	1.9 ± 0.6	0	1.8	6.7 ± 1.7	9.0 ± 3.0
3.0→3.5	1.9 ± 0.6	0	0.8	0.0 ± 0.0	3.0 ± 1.7

[a]The errors are statistical based on the number of observed ''tagged'' Bi decays. A systematic error of about ±10% can be expected for ^{212}Bi background because of uncertainty in the detection efficiency of ''tagged'' events with fast clock time <0.2 μs, and a systematic error of about ±15% can be expected for ^{214}Bi background because of uncertainty in the detection efficiency for the α's in ''tagged'' events.

TABLE VI. Energy-weights=$\mathcal{P}_j$, $j=1\rightarrow3$ for the 12 events with energy between 2.5 and 3.5 MeV.

Event	E (MeV)			
(i)	$E(i)$	$\mathcal{P}_1$=signal	$\mathcal{P}_2=^{212}$Bi	$\mathcal{P}_3=^{214}$Bi
1	2.502	1.165	1.0	5.952
2	2.511	1.199	1.0	5.739
3	2.532	1.282	1.0	5.257
4	2.538	1.307	1.0	5.123
5	2.571	1.448	1.0	4.417
6	2.591	1.539	1.0	4.015
7	2.644	1.797	1.0	3.042
8	2.662	1.889	1.0	2.742
9	2.726	2.223	1.0	1.802
10	3.070	0.0	1.0	0.0
11	3.092	0.0	1.0	0.0
12	3.226	0.0	1.0	0.0
Best fit, s=0.0, ^{212}Bi=b_1=4.1, ^{214}Bi=b_2=7.9				

The Bayesian confidence level (C.L.) of an upper limit l on s is then defined to be the probability that $s<l$ and, rewriting f_b as $b/(b+s)$ and f_s as $s/(b+s)$, can be obtained from the expression

$$\text{C.L.}=\int_0^l \mathcal{L}_n ds=\frac{\int_{s=0}^{s=l} e^{-s}\Pi_{i=1}^{n}[b\mathcal{P}_b(E_i)+s\mathcal{P}_s(E_i)]ds}{\int_{s=0}^{\infty} e^{-s}\Pi_{i=1}^{n}[b\mathcal{P}_b(E_i)+s\mathcal{P}_s(E_i)]ds}.$$

If b is known, this equation for C.L. can be integrated numerically for various values of l until a value of l is found which gives the desired confidence level. Figure 17 shows the value of $\mathcal{L}_n$ and C.L. vs the signal s for the best fitted values of the backgrounds ^{212}Bi=4.1 events and ^{214}Bi=7.9 events. This gives 1.85 (3.63) events for a Bayesian C.L. limit of 68% (90%). Table VII shows the dependence of the numbers of signal events, for a C.L. of 68%, upon the two Bi backgrounds.

From these confidence limits, calculated half-life limits can be obtained for the $0^+\rightarrow0^+$ neutrinoless double-β decay of 0.22×10^{23} yr (68%) and 0.11×10^{23} yr (90%). This is the best $0^+\rightarrow0^+$ result published to date for ^{100}Mo.

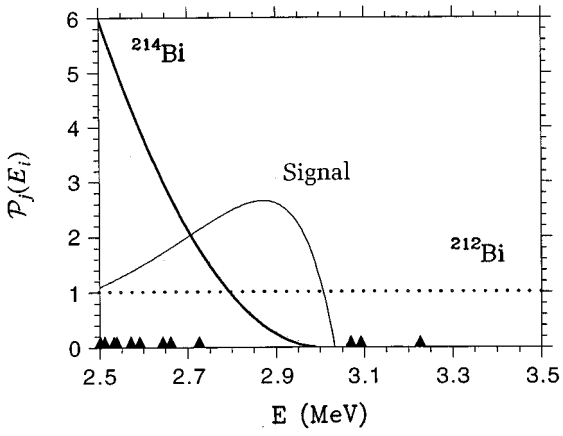

FIG. 15. The energy weights $\mathcal{P}_j(E_i)$, described in Sec. VI A for event energy (E_i) between 2.5 and 3.5 MeV. The shape of the signal ($\mathcal{P}_1$) (light curve) is obtained by Monte Carlo simulation. The shape of the ^{212}Bi background ($\mathcal{P}_2$) (dotted line) is from events ''tagged'' by the fast clock. The shape of the ^{214}Bi background ($\mathcal{P}_3$) (heavy curve) is obtained by Monte Carlo simulation and also from the events ''tagged'' by the fast clock. For details see the text. The areas under the curves have been normalized to 1.0 for the energy region $2.5 < E < 3.5$ MeV. The energies of the 12 events observed are also shown as solid triangles on the E axis.

B. Fits to the energy spectra of double-β-decay ''candidates'' for two-neutrino and $0^+\rightarrow2^+$ zero-neutrino decays

Least square fits using 50 keV bins were made to the ''candidate'' energy spectrum for stack 2 [Fig. 18(a)], and also to the corresponding data from stack 1 [Fig. 18(b)], which were already shown in 10 keV bins in Figs. 9(a) and 9(b). For stack 2 the energy region fitted was 1.9 to 2.5 MeV, and for stack 1 was 2.0 to 2.6 MeV. The energy limits chosen for the comparison of stack 1 with stack 2 data were determined by comparing the energy losses of monoener-

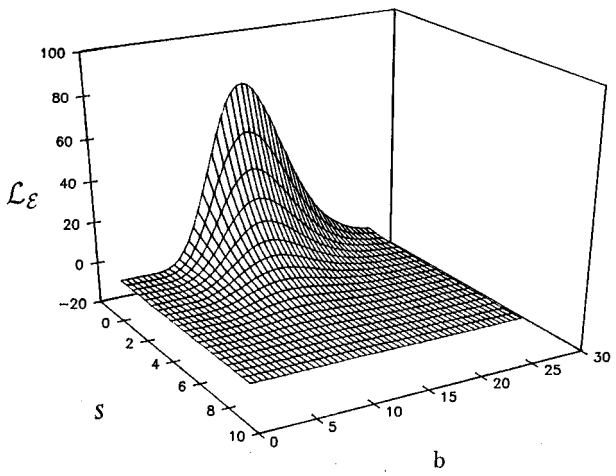

FIG. 16. A 3D plot of the extended likelihood function defined in the text vs the signal (s) and background (b).

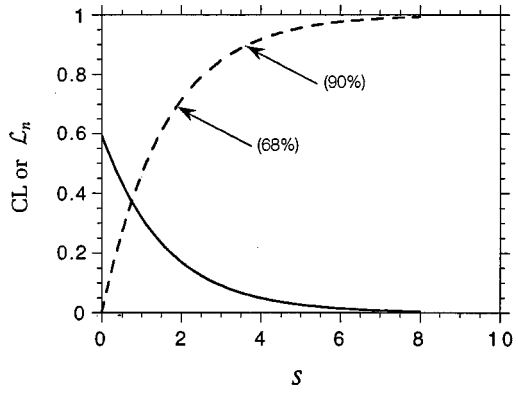

FIG. 17. The normalized extended likelihood function ($\mathcal{L}_n$) (solid curve) and the Bayesian confidence level (C.L.) (dashed curve) defined in the text vs signal (s). The 68% and 90% limits are indicated by arrows.

getic Monte Carlo generated electrons in the two stacks. For fits to stack 2 data, 8 decay channels were considered: three possible double-β-decay signals [i.e., 0ν ($0^+\rightarrow 0^+$), 0ν ($0^+\rightarrow 2^+$) and 2ν], and five possible backgrounds i.e., ^{212}Bi, ^{214}Bi or ^{208}Tl β decays, and the interaction of high energy γ's from ^{214}Bi and ^{208}Tl [$E(\gamma)=2.448$ and 2.614 MeV respectively]. For stack 1 data, only the five backgrounds were considered. The shapes of the energy spectra were parametrized. (See Appendix B for details.)

For all fits to the experimental data, the contribution from neutrinoless double-β-decay transition $0^+\rightarrow 0^+$, and ^{212}Bi and ^{208}Tl β decays were set to zero because the maximum likelihood fit to stack 2 data above $E=2.5$ MeV (described in Sec. VI A) showed that these contributions were very small. Preliminary least squares fits to the data below 2.5 MeV indicated that the contribution from the interactions of the 2.448 MeV γ's from ^{214}Bi was also small and could be set to zero, but that the contributions from ^{214}Bi beta decays and ^{208}Tl γ interactions were large and had to be included in the fits for both detector stacks.

The results of the best fits are shown in Table VIII and Fig. 18. In these fits the decay channels indicated are allowed to vary freely and all other channels are set to zero. The fit to stack 2 data for $1.9<E<2.5$ MeV is a good fit with no contribution from a $0^+\rightarrow 2^+$ signal. A fit for $2.1<E<2.5$ MeV which includes a $0^+\rightarrow 2^+$ signal (not shown) improves the fit for this small energy region but cannot explain the data below 2.1 MeV. The fit for stack 1 is not as good as for stack 2; however, most of the χ^2 sum (8.63 out of 13.67) comes from the two bins between 2.3 and 2.4 MeV. (This apparent structure is probably a statistical fluctuation because it is too narrow to be a true physical effect.)

TABLE VII. The number of signal events that give a 68% confidence limit as a function of ^{212}Bi (b_1) and ^{214}Bi (b_2) background events.

		^{214}Bi(b_2)		
		7.5	7.9	8.3
^{212}Bi(b_1)	3.7	1.91	1.86	1.82
	4.1	1.89	1.85	1.81
	4.5	1.88	1.83	1.80

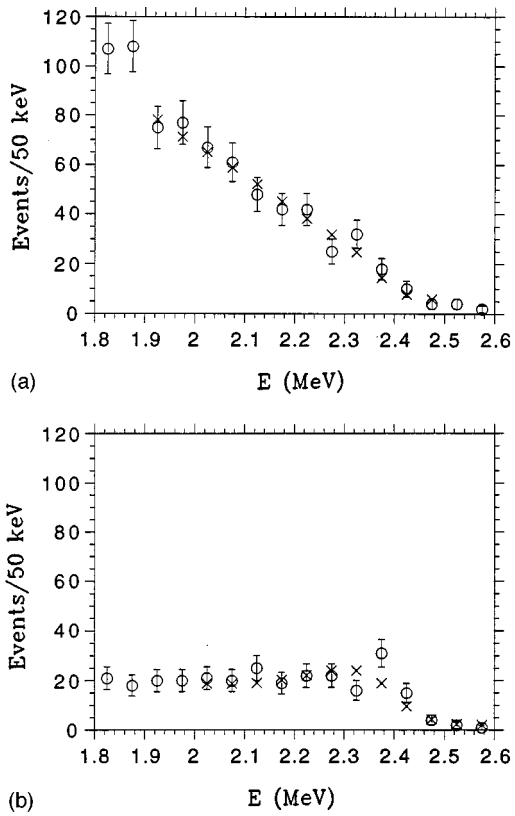

FIG. 18. The events remaining after all cuts in (a) stack 2 and (b) stack 1. These data (circles) are the same as those in Fig. 11 but replotted in 50 keV bins. The crosses are the best least square fits described in the text and Table VIII.

Figure 18 shows that the shapes of the experimental energy spectra from stack 1 and stack 2 are very different. The fits show that a contribution from two-neutrino double-β-decay in stack 2 describes the difference very well. Although comparison between the absolute number of events in stack 2 and stack 1 is difficult because of the very different geometries (foils vs no foils), the contribution of ^{214}Bi β decays in stack 2 is nearly 2/3 from the foils and 1/3 from the surroundings. The number of Tl γ interactions approximates the expected number, since the foils introduce 10% additional material.

The best fit value of the number of 2ν double-β-decay events (s_2) in the energy region $1.9<E<2.5$ MeV is 175.8 ± 40.1. Then the half-life for the two-neutrino double-β decay of ^{100}Mo is given by

$$t_{1/2}=\frac{\ln(2)\times\epsilon_2\times T\times N_a}{s_2},$$

where ϵ_2=detection efficiency=0.012 (from the Monte Carlo simulation), T=live-time=0.2664 mole yr, and N_a=Avogadro's number, giving $t_{1/2}=0.76^{+0.22}_{-0.14}\times 10^{19}$ yr. This value is in reasonable agreement with the latest measurements, i.e., $t_{1/2}=0.33^{+0.2}_{-0.1}\times 10^{19}$ to $1.16^{+0.34}_{-0.08}\times 10^{19}$ years [15]. Also see Table I.

Our results show no evidence of a $0^+\rightarrow 2^+$ transition in neutrinoless double-β decay.

TABLE VIII. Fits to the low-energy data from stack 2 (foils) and stack 1 (no foils).

Stack	E region (MeV)	Channel filled	Number of events	Error	χ^2	N_{DF} [a]	C.L. [b]
2	1.9 → 2.5	^{214}Bi	168.9	± 42.6	7.12	9	0.645
		Tl γ	149.4	± 46.4			
		2ν	175.8	± 40.1			
1	2.0 → 2.6	^{214}Bi	55.4	± 16.9	13.67	10	0.189
		Tl γ	126.9	± 19.4			

[a] N_{DF} is the degrees of freedom of the fit.
[b] C.L. is the confidence level of the fit.

VII. CONCLUSION

A limit on the effective Majorana neutrino mass $\langle m_\nu \rangle$ can be estimated from the relationship between the half-life of a double-β decay ''candidate'' isotope and the mass of the neutrino which has the form [16]

$$\frac{1}{\tau^{0\nu}_{1/2}} = \mathcal{G}(Q,Z)\left|M_{\mathrm{GT}} - \frac{g_V^2}{g_A^2} M_F\right|^2 \langle m_\nu \rangle^2,$$

where $\mathcal{G}(Q,Z)$ is a numerically integrated phase space factor which depends on the nuclear decay energy Q and the isotope atomic number Z, M_{GT} and M_F are the Gamow-Teller and Fermi matrix elements for the decay, and g_V and g_A are vector and axial vector coupling constants. Values of $\mathcal{G}(Q,Z)$ have been calculated for various isotopes of interest by Doi *et al.* [17]. The quantity $|M_{\mathrm{GT}} - (g_V^2/g_A^2)M_F|$ has been calculated by Engel for ^{100}Mo [16]. Using these results, the half-life which corresponds to an effective Majorana mass of 1 eV for neutrinoless double-β decay in ^{100}Mo is 1.9×10^{24} yr. This result can then be scaled by the 68% half-life limit obtained in this experiment to give an upper limit of 9.3 eV on the Majorana neutrino mass.

It should be emphasized, however, that this mass estimate is both model dependent and sensitive to the approximations used to calculate the matrix elements. Because these matrix elements are not precisely known, it is important to compare mass limits derived from lifetime limits for several ''candidate'' isotopes. Published limits on the Majorana neutrino mass derived from germanium and xenon experiments vary from less than 1.0 eV to 5.0 eV, the best germanium limit being the most restrictive [18,19]

ACKNOWLEDGMENTS

We are indebted to the Hecla Mining Co. and to the ASARCO Mining Co. for access to the Consolidated Silver Mine. We thank Philippe Eberhard, Don Groom, Gerry Lynch, Mahiko Suzuki, A. Carl Helmholz, and Michael Moe for valuable discussions and reference information. We thank Alan Smith for radioactive assays and essential advice in our selection of clean materials. We also thank James VanKuiken for a long history of support underground, Michael Long and Chilton Gregory for technical support, Lydia Young for suggesting making clip detector contacts, and Ju Kang, Benjamin Brown, and Kevin Watts for taking shifts underground at the mine in Idaho. Thanks to Jeanne Miller for the final editing of the manuscript. This work was supported by U.S. Department of Energy Contracts and Grants DE-AC07-76ID0-1570, DE-AC03-76SF00098, DE-FG04-88ER40395, DE-FG05-88ER75444, and DE-FG02-90ER40553.

APPENDIX A: BACKGROUND STUDY, COMPARISON OF THE DATA FROM STACK 1 AND STACK 2 FOR E27-30

The data obtained in Experiments 27-30 (live-time =3286.7 hrs) were studied in detail to determine possible sources of backgrounds in the double-β-decay ''candidate'' sample. In particular, comparison of event rates in stack 1 versus stack 2 (detectors 76-138) for ''tagged'' Bi decays, and multi-α sequences were made. The cuts imposed on the events for this study were minimal. Electronic noise was removed by cuts (1a) described in Sec. III. In addition, events ''tagged'' by the fast clock were identified as ^{212}Bi decays if the fast clock time was between 0.2 and 2 μs, and as ^{214}Bi decays for times between 20 μs and 1 msec. For multi-α-decay sequences, each one detector event in the sequence was required to have energy greater than 2 MeV in the same or adjacent detectors. The number of ''tagged'' β decays and multi-α sequences detected are shown in Table IX.

For the ''tagged'' Bi, the relative number of events are as expected; i.e., the number of events in stack 2, which contained the ^{100}Mo foils, are greater than in stack 1, indicating the introduction of both ^{212}Bi and ^{214}Bi in the foils. The increase is larger for ^{214}Bi than for ^{212}Bi.

However, the relative numbers of 2 and 3 α sequences in the two stacks are unexpected since the α sequences detected in stack 2 are often less than in stack 1. The lower part of the ^{232}Th decay chain should be in equilibrium even after chemical separation of the ^{100}Mo because the half-lives in this part of the chain are 11 hours or less (see Fig. 6). Thus the decrease rather than increase in the number of multi-α sequences observed in stack 2 shows that even though the radioactivity has been increased by the introduction of the foils, the Mo has reduced the detection efficiency for α's by absorbing and degrading them.

If the α's come from the source foils, all 2 or 3 α's detected in a sequence should be in one detector because the thickness of a foil (34 mg/cm^2) is greater than the range of any of the α's. If, however, the source nucleus is not in a source foil but is situated somewhere close to the sensitive

TABLE IX. Background events observed in experiments 27 → 30.

(a) ''Tagged'' events			
	Stack 1	Stack 2	Total
^{212}Bi ($0.2< t_{\text{fast}} < 2$ μs)	73	186	259
^{214}Bi ($20< t_{\text{fast}} < 1000$ μs)	170	809	979
(b) α sequences			
	Stack 1	Stack 2	Total
Three sequential α events			
All	56	30	86
Energy in one detector	17	18	35
Energy in two adjacent detectors	39	12	51
Two sequential α events			
All	104	100	204
Energy in one detector	60	78	138
Energy in two adjacent detectors	44	22	66

regions of two adjacent detectors, and if each detector has the same efficiency for detecting α's of the same energy, then for two α sequences there should be the same number observed in one detector as in two detectors, and, for three α sequences three times as many detected sequences in two detectors as in only one detector, i.e., 3/4 vs 1/4 of the total. Two and three α sequences are observed in adjacent detectors in stack 2, which shows that many of the source nuclei are not in the foils. Thus backgrounds from the ^{232}Th decay chain must come from both the foils and from the surroundings. A probable source of the ^{232}Th decay chain background is the Ti clips used to make electrical contact with the detectors. Activity of 4 ppb was found by low-background counting of the Ti material before it was made into contacts and placed into the experiment. This level of contamination explains the number of events observed.

APPENDIX B: FITS TO THE MONTE CARLO GENERATED ENERGY SPECTRA

Least squares fits were made to the Monte Carlo generated signal and background energy spectra described in Sec. IV.

1. Signal

(1) Neutrinoless double-β decay. The form of the least square fits to the generated data for $0^+ \rightarrow 0^+$ with $2.00 < E < 2.99$ MeV and for $0^+ \rightarrow 2^+$ with $2.00 < E < 2.46$ was

$$y(E) = a_1(1. - e^{(E-a_2)/a_3})e^{(E-a_2)/a_4}.$$

Between 2.99 and 3.03 MeV, the Q value of ^{100}Mo, the $0^+ \rightarrow 0^+$ data was fit to a curve of the form

$$y(E) = a_{11}e^{(a_{12}-E)/a_{13}}.$$

Above 2.46 and below 2.85 MeV, the $0^+ \rightarrow 2^+$ data were fit to the straight line

$$y(E) = a_{12}E + a_{11}$$

The values of the a parameters for these fits are given in Table X and the fitted curves are shown in Figs. 12(a) and 12(b).

(2) Two-neutrino double-β decay. In the energy region $1.7 < E < 2.4$ MeV, a good fit to the generated spectrum of the two neutrino double-beta-decay spectrum of ^{100}Mo was given by the quadratic

$$y(E) = 891.0 - 695.0E + 135.0E^2$$

The number of generated events in this energy region which satisfied all the cuts was 556. The fitted curve is shown in Fig. 12(c).

2. Backgrounds

In the energy region above 2.0 MeV, the major backgrounds came from the following sources: (a) ^{214}Bi β decay, (b) ^{208}Tl β decay, (c) interactions of 2.448 MeV γ's from ^{214}Bi, (d) interactions of 2.614 MeV γ's from ^{208}Tl.

The shape of the fit to the ^{214}Bi β-decay data [Fig. 13(b)] was obtained by fitting a spectrum of the form

$$y(E) = 72.0(E - 3.0)^2$$

to Monte Carlo generated data. This could then be compared to the actual ^{214}Bi β decays ''tagged'' by α particles that were obtained in the experiment. Although there were only

TABLE X. Values of the parameters for the fits to signal spectral shapes.

	$0^+ \rightarrow 0^+$	$0^+ \rightarrow 2^+$
a_1	772.5682	420.9500
a_2	3.0157	2.4662
a_3	0.1505	0.0668
a_4	0.2909	0.3207
a_{11}	102.3545	190.0615
a_{12}	2.9902	−66.9462
a_{13}	0.0079	

TABLE XI. Parameters of the γ interaction spectral shapes.

	^{214}Bi Stack 1	^{214}Bi Stack 2	^{208}Tl Stack 1	^{208}Tl Stack 2
x_1	25.398	16.014	31.064	40.460
x_2	0.978	0.127	1.093	0.216
x_3	4.497	1.112	1.336	0.649
x_4	0.180	0.168	0.156	0.170
x_5	0.037	0.027	0.030	0.022
E_1	1.543	−3.290	1.504	1.124
E_2	2.294	1.943	2.346	2.095
E_3	2.180	2.189	2.401	2.364

13 ''tagged'' ^{214}Bi events in the energy region between 2.0 and 3.0 MeV, this parametrization represented these data quite well.

The shape of the fit to the ^{208}Tl β-decay spectrum for energies between 2.0 and 3.5 MeV to Monte Carlo generated data was well approximated by the following straight line:

$$y(E) = -17.2E + 60.316.$$

Fits were also made to Monte Carlo generated data for the ^{208}Tl 2.615 MeV γ and for the ^{214}Bi 2.445 MeV γ for both the detector stack 1 which contained no molybdenum foils and detector stack 2 which did. All these fits, which were a parametrization of the Klein-Nishina formula for Compton scattering into a finite resolution detector, had the form

$$y(E) = x_1(1 + x_2(E - E_1) + x_3 e^{-[(E-E_2)/x_4]^2}) \times f_{\text{cut}}$$

with a cutoff factor of the form

$$f_{\text{cut}} = \frac{1.0}{(1. + e^{(E-E_3)/x_5})}.$$

Parameters of these fits are given in Table XI and the fitted curves are shown in Figs. 14.

APPENDIX C: PREDICTED BACKGROUNDS IN THE ''CANDIDATE'' SAMPLE

To predict the number of background events in the sample of double-β-decay ''candidates'' from E27-31 in the energy region $2.0 < E < 3.5$ MeV, the observed Bi decays ''tagged'' by the fast clock, and the Monte Carlo generated ^{208}Tl events have to be normalized to the ''candidate'' sample. This is difficult because many of the background source nuclei are somewhere external to the foils, and their locations, and thus the detection efficiency of their decays, are unknown.

Detailed studies of backgrounds in the experiment were made using data from E27-30. To normalize these data to the sample for E27-31, the ratio of live-times, E27-31/E27-30, is 1.17.

1. ^{212}Bi

The transition energy for this β decay is 2.25 MeV, and Monte Carlo simulation of decays from the foils predict observed β energies less than 2.0 MeV. So the detection of either a ''tagged'' or ''untagged'' ^{212}Bi decay for energies, $2.0 < E < 3.5$ MeV, requires that some additional energy in the ADC's is due to the α from the fast decay of the ^{212}Po daughter ($t_{1/2} = 0.3$ μs). The gate time of the ADCs is 2 μs which gives the upper limit in time for acceptance of ''tagged'' ^{212}Bi decays. Study of the recorded fast clock time of ''tagged'' events shows that the trigger system does not recover for at least 0.1 μs and is not completely recovered until 0.2 μs. For the energy region $2.0 < E < 3.5$ MeV and after all the cuts made to select double-β-decay ''candidates'' (except the fast ''tag'' cut), there are ten ''tagged'' events with observed fast clock time between 0.2 and 2 μs [Fig. 11(a)], and three with time between 0.13 and 0.2 μs. These 13 events have a flat energy distribution. Assuming that the efficiency for detecting a second trigger is 100% for $0.13 < t_{\text{fast}} < 0.2$ μs, the efficiency in this time interval is 0.73. Then the ratio ''untagged''/''tagged'' $= (1.0 - 0.73)/0.73 = 0.37$, independent of both the β and α geometric detection efficiencies. The overall normalization to obtain ''untagged'' ^{212}Bi decays for E27-31 $= 0.37 \times 1.17 = 0.43$, giving the estimated number of ''untagged'' ^{212}Bi decays with energy between 2.0 and 3.5 MeV, with flat energy distribution, of 1.9 ± 0.6 events/500 keV. The quoted error is statistical.

2. ^{208}Tl

A detailed study of the 2 and 3 α-decay sequences and the ''tagged'' ^{212}Bi events indicate that there were probably less than 500 ^{208}Tl decays in E27-30. If the decaying nuclei are assumed to be in the foils which are snugly situated between the detectors, detection efficiencies derived from the 20 000 Monte Carlo generated events [Fig. 11(c)] can be used to predict a maximum number of observed ^{208}Tl decays for $2.5 < E < 3.5$ MeV of about 2.6 events. However, sources outside or at the edges of detectors, and, in particular, in the suspected Ti contact clips should have much smaller detection efficiencies than for sources in the foils because the β and γ's from the ^{208}Tl decay can easily go out of the detector stack. The transition energy $^{208}\text{Tl} \rightarrow {}^{208}\text{Pb}$ is 5.0 MeV, but the decay goes via the first excited state of ^{208}Pb at 2.614 MeV 99.8% of the time, and since about 90% of the γ's will Compton scatter in Si, a Compton edge at 2.4 MeV should result. The most likely β transition energies are 1.8 MeV (51%), 1.5 MeV (22%), and 1.3 MeV (23%), and these transitions are accompanied by additional γ's. Thus, to observe more than 2.4 MeV in a ''candidate'' event requires the detection of at least two particles (i.e., either the β and a γ interaction, or two γ interactions) in the sensitive regions of two or three contiguous detectors. Thus the minimum number of observed ^{208}Tl background from nuclei situated outside the foils is very small and probably zero.

3. ^{214}Bi

This background from the ^{238}U decay chain is observed as either events ''tagged'' by the fast clock or ''untagged'' events. The α ''tag'' is not detected if the α does not escape from the source material, or, if it escapes, it does not enter the sensitive region of a detector with enough energy to cause a second trigger.

The time detection efficiency for observing a ^{214}Po α

decay within the time interval 2 μs $\rightarrow$ 1 ms ($T_{1/2}=165$ μs) is 0.98. The geometric detection efficiency for ''tagging'' the β decay with the subsequent α decay depends strongly on assumptions about where the decay source is situated.

(a) If the source is distributed uniformly in the Mo powder then the probability that the α exits the foil can be calculated, i.e., $P=R/2t=0.33$, where R=the range of the 7.7 MeV $\alpha=23.07$ mg/cm^2 and t=the thickness of the foil= 34.6 mg/cm^2.

(b) If the source is somewhere external to the foils, then the α detection efficiency may be much less than 0.33 because even if the α exits the source material it may not enter the sensitive region of a detector. Additional studies of the ^{214}Bi backgrounds show that 1/2 to 2/3 of this contamination is in the foils.

If a detection efficiency for the α of 0.25 is used, the ratio ''untagged''/''tagged''$=(1-0.25)/0.25=3.0$, and normalization to E27-31$=3.0\times1.17=3.5$. There are two ''tagged'' events with $2.5<E<3.0$ MeV and 13 with $2.0<E<2.5$ MeV. The shape of the ^{214}Bi spectrum from Monte Carlo studies, normalized to 15 events, gives 1.9 and 13.1 events, respectively, in good agreement. Then the factor of 3.5 predicts 6.7 $\pm$ 1.7 and 45.9 $\pm$ 11.9 respectively for the ''untagged'' background in the double-β-decay ''candidate'' sample from E27-31.

The predicted number of background events from ^{212}Bi, ^{214}Bi, and ^{208}Tl β decays in the double-β-decay ''candidate'' sample are shown in Table V. The quoted errors in this table are statistical derived from the number of observed ''tagged'' decays. The estimated systematic errors for ^{212}Bi and ^{214}Bi contributions are $\pm$ 10% and $\pm$ 15% respectively.

[1] J. Schecter and J. W. F. Valle, Phys. Rev. D **25**, 2951 (1982).
[2] B. Kayser, Nucl. Phys. **A546**, 399c (1992).
[3] M. Alston-Garnjost *et al.*, Phys. Rev. Lett. **63**, 1671 (1989).
[4] M. Alston-Garnjost *et al.*, Phys. Rev. Lett. **71**, 831 (1993).
[5] S. R. Elliott *et al.*, J. Phys. G **17**, s145 (1991).
[6] M. Alston-Garnjost *et al.*, Nucl. Instrum. Methods **A271**, 475 (1988).
[7] Micron Semiconductor, 126 Baywood Ave., Longwood, FL 32750.
[8] J. M. Krivicich, ''A New Limit on the Neutrinoless Double Beta Decay of ^{100}Mo,'' Ph.D. thesis, Report No. LBL 25233, 1988 (unpublished).
[9] C. M. Lederer *et al.*, *Table of Isotopes* (Seventh Ed.) (Wiley New York, 1978).
[10] R. Brun *et al.*, GEANT 3 Users Guide, CERN Data Handling Division Report No. DD/EE/84-1, 1984, revised 1987 (unpublished).
[11] B. L. Dougherty, ''An Experimental Investigation of Double Beta Decay of ^{100}Mo,'' Ph.D. thesis, Report No. LBL 26303, 1988 (unpublished).
[12] L. Lyons, *Statistics for Nuclear and Particle Physicists* (Cambridge University Press, Cambridge, England, 1986), p. 101.
[13] F. James *et al.*, MINUIT Function Minimization and Error Analysis, Long Write-Up, CERN, Geneva 1989, revised 1992.
[14] V. Innocente and L. Lista, Nucl. Instrum. Methods **A340**, 396 (1994).
[15] M. Moe and P. Vogel, Annu. Rev. Nucl. Part. Sci. **44**, 247 (1994).
[16] J. Engel *et al.*, Phys. Rev. C **37**, 731 (1988).
[17] M. Doi *et al.*, Prog. Theor. Phys. Suppl. **83**, 1 (1985).
[18] M. K. Moe, Int. J. Mod. Phys. E **2**, 507 (1993).
[19] H. V. Klapdor-Kleingrothaus *et al.*, Nucl. Phys. B, Proc. Suppl. **31**, 72 (1993).